Research Report 114

NOVEMBER 1963

Properties of Ice

Part II

by Paul R. Camp

U.S. ARMY MATERIEL COMMAND
COLD REGIONS RESEARCH AND ENGINEERING LABORATORY
Hanover, New Hampshire

Table of Symbols (Cont'd)

ρ_p = Integrated surface reflection for perfect crystal

σ = Conductivity where there is no ambiguity between a-c conductivity (σ_{ac}) and d-c conductivity (σ_{dc})

τ = Relaxation time

ϕ = Angle between electric vector and plane of reflection

ω = Angular frequency, radians per second.

RESEARCH REPORT 114

Errata

P. 8, line 27: for 30 K read 30 kilovolt

P. 9, eqs. 9 and 11: for ρ_m and R_m substitute ρ_M and R_M

P. 14, line 2: beginning "In the . . . ." Omit this sentence.

P. 20, line 2: after "similar," insert "to"

P. 21, line 6: for "e" substitute "E"

P. 31, line 12: for R substitute R_s

P. 36, line 20: for σ substitute σ_s

Table of Symbols

A = Angstrom unit (or undetermined constant)

A_0 = Relation defined, p. 5, eq. 4

c = Velocity of light

C = Capacitance, subscripts s, p, o, ∞ indicate series, parallel, zero frequency, microwave frequency, respectively

d = Spacing between reflecting planes (in Bragg equation)

e = Base of natural logarithm, or charge of electron.

E = Electric field, or activation energy

E_0 = Energy required to create one, or a mole, of Bjerrum defects (as the equation demands)

f = Frequency

f_n = Frequency at which the imaginary part of the dielectric constant $1/(\omega R_p)$ is a maximum

F = Geometrical structure factor

g = Coefficient of secondary extinction

h = Planck's constant

J = The Bessel function

Table of Symbols (Cont'd)

k = Boltzman's constant, or, where obvious, an undetermined constant.

K = Kelvin temperature

m = Mass of electron

n = Order of Bragg reflection

Q = Relation defined on p. 6, eq. 5

Q' = $Q\, f(A_0)$, $f(A_0)$ defined on p. 5, eq. 3

r = Resistance (input resistance of oscilloscope)

R = Gas constant, or, where obvious, resistance

R_{dc} = D-C resistance

$R_H{}^{\theta}$ = Relation defined on p. 5, eq. 1

t = Time

t_0 = Thickness of a mosaic block

T_0 = Thickness of crystal

V = Volume of the unit cell, or voltage

y = Complex admittance

ϵ' = Real part of dielectric constant. Subscripts o, ∞ refer to d-c and microwave values, respectively.

ϵ'' = Imaginary part of dielectric constant

θ = Angle between normal to crystal and incident beam

θ_B = Bragg angle

θ_D = Debye temperature

λ = Wavelength

μ = Micron = 10^{-4} cm

μ_0 = Linear absorption coefficient for X-rays

ρ_M = Integrated surface reflection for mosaic crystal

PREFACE

This report on Contract No. DA-11-190-ENG-68 with the Department of Physics of the Polytechnic Institute of Brooklyn is a final report for the period 31 September 1959 through 31 July 1961 during which time the contract was under the direction of Dr. Paul R. Camp.

Many people have contributed to the technical work described in this paper. Dr. Alfred Zajac has been a principal contributor in the field of X-ray crystallography. Others who have worked in one or more of the areas covered are Thomas Ammarato, Thomas Acquaviva, James Benson, Marvin Fastman, Vito De Palma, Ira Gilbert, Frank Goldner, Gerald Minerbo, Janett Rosenberg, Edward Saccocio, Leslie Spaiser, and Samuel Tauster.

Mr. Kermit Hale, Mr. Edward Podlasiewicz and Mr. Bernard Miller helped in the construction of apparatus and Mrs. Rosemarie Suchman worked in connection with the manuscript and also assisted in making the day-to-day operations of the project go smoothly.

This report has been reviewed and approved for publication by Headquarters, U. S. Army Materiel Command.

W. L. NUNGESSER
Colonel, CE
Commanding
USA CRREL

Manuscript received 17 July 1962

Department of the Army Project 8-66-02-400

CONTENTS

ILLUSTRATIONS

CONTENTS (Cont'd.)

SUMMARY

Modifications are reported of a previously described apparatus for the preparation of single crystals of pure and doped ice. Some results of using this apparatus to grow crystals of several crystallographic orientations are discussed. An effect of an electric field on the nucleation of ice at a metal-water interface is described.

Various X-ray techniques for investigating the quality of ice crystals are discussed and experimental results of applying them to Alaskan Glacier crystals are given. Among the techniques used are the measurement of the half width of the reflection curve, the integrated reflecting power of a Laue reflection, studies with polarized X-rays and a transmission technique due to Lang. The thermal motion of ice molecules in a direction perpendicular to the c-axis and the temperature dependence of the lattice parameters of ice have been measured by X-ray techniques.

Dielectric relaxation and electrical conductivity of ice are discussed. Experiments have been performed to determine the effect of length of the sample and to study the effect of small amounts of NH_4F as a substitutional impurity. Special attention is given to long period dielectric processes. At least two such processes seem to be present, one which dominates the first 3 to 30 seconds of discharge and the other which determines the long time behavior. The possibility of altering the conductivity and dielectric relaxation of ice by optical generations of Bjerrum defects is explored and experiments to test this possibility are reported.

PROPERTIES OF ICE, PART II

by

Paul R. Camp

SINGLE CRYSTAL PREPARATION

Crystal growth

A crystal-growing apparatus was described in an earlier report (Brill and Camp, 1961, p. 1-7). This apparatus consisted of a nearly horizontal arrangement of cold and hot zones through which was passed a sealed tube containing a seed crystal, melt liquid, and possibly polycrystalline ice to replenish the melt in a suitably programmed way. This arrangement is flexible, allows the use of a sealed system, and permits programmed doping of the ice with desired impurities. Figure 1 is a diagram of the apparatus showing recent modifications. The principle changes are the addition of a long hot-wire heater and modification of the end plug.

The hot wire is merely a long, finely wound spiral heater laid along the bottom of the V-groove which carries the crystal-growing tube. It was added so that, when desired, the whole region from the crystal to the end plug could be maintained liquid. This has simplified the procedure for growing crystals of pure ice and helped in experiments which require remelting of the sample. A very simple and fairly satisfactory method of growing single crystals of pure ice has evolved since the installation of this heater. A Lucite tube is nearly filled with water at 1C and suitably seeded. It is placed so that the end of the hot wire coincides with the liquid-solid interface. The tube is rotated and pushed off the wire at the desired growth rate. If the room temperature is sufficiently low and constant, the heater wire may be adjusted so that the liquid-solid interface remains very nearly at the end of the hot wire. For a room temperature of -10C, a heater power of about 20 watts per centimeter of heater length has been satisfactory. A lower room temperature is desirable. It should be emphasized that an accurately controlled growth rate requires accurately controlled temperatures and a large temperature gradient in the vicinity of the liquid-solid interface.

The modification of the end plug consisted simply of cutting a flange on it to fit the tube and cementing it on with epoxy. Previously it had been demountable with a screw thread and an O-ring assembly. Abandonment of the demountable feature eliminates a troublesome mechanical structure and an element which is difficult to clean. However, the most important advantage is that now crystals can be stored without removing them from the tube in which they are grown and can be dissected while still protectively enclosed in Lucite.

A serious problem in growing ice crystals is caused by dissolved gases. These cause bubble formation when the rate of growth exceeds a few millimeters per hour. In the past, efforts have been made to eliminate the dissolved gases by pumping the system down to the vapor pressure of water at 1C and then sealing it off. This has presented some difficult problems in technique and has been only partially successful because no system we have built has been completely vacuum tight.

Another partial cure is to boil the water, fill and seal the tube while the water is still very hot, and then seed it after it cools. This reduces the dissolved gas content but does not eliminate it.

Recently we have experimented with flushing the tube with Freon 12 and then filling the tube with hot water in an atmosphere of Freon. The results were disappointing and suggest that the Freon is more soluble in water than had been supposed. Bubbles still form when the growth rate exceeds 3 mm/hr.

A number of crystals both pure and doped have been grown with this apparatus. Usually the seed crystal was oriented so that growth took place either along or perpendicular to the c-axis. Occasionally, however, by some accident of technique a new

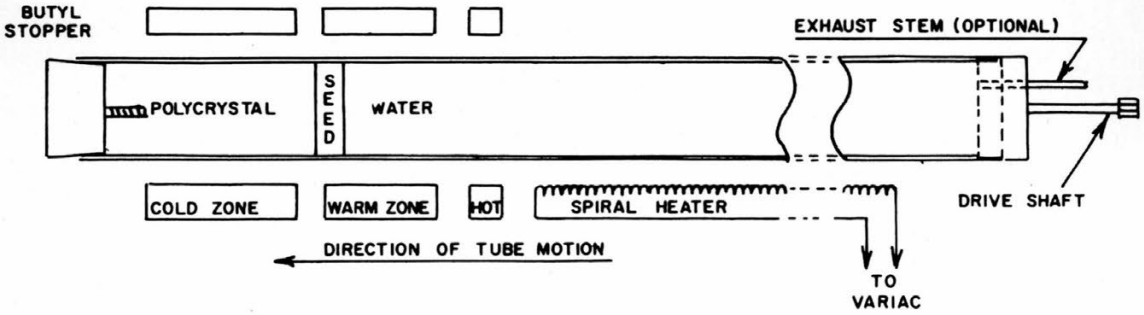

Figure 1. Drawing of crystal growing apparatus.

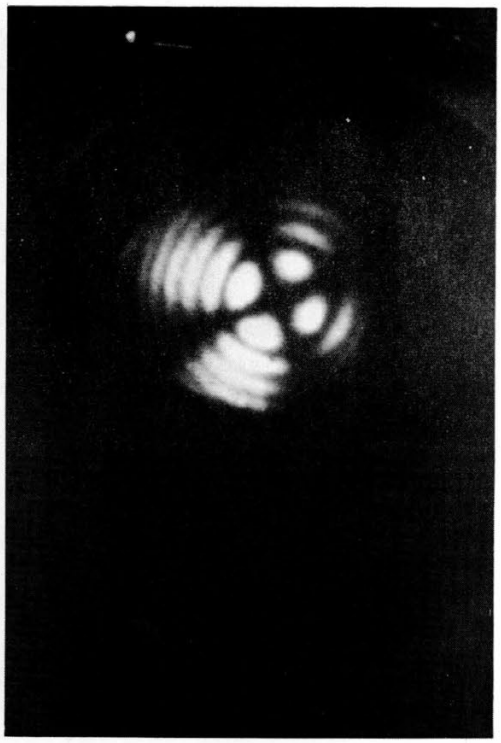

Figure 2. Photograph of the brush figure produced when ice is viewed along the c-axis using highly divergent polarized light. The crystal used here was grown along the (212) direction.

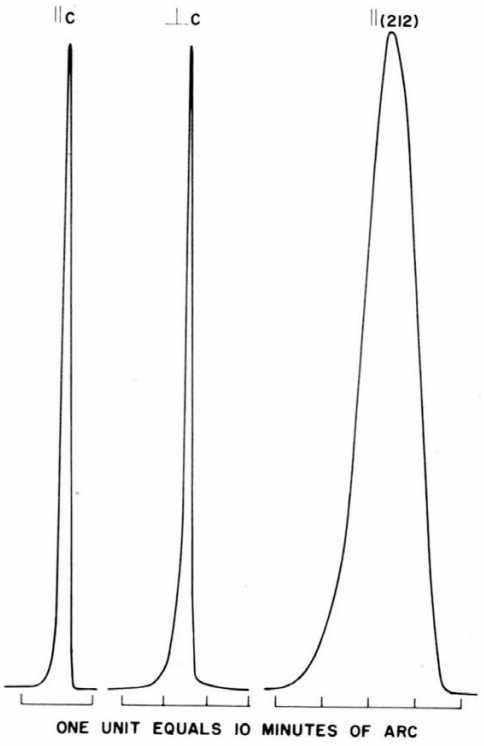

Figure 3. X-ray line widths for (002) Bragg reflection for crystals grown along c-axis, perpendicular to c-axis, and along the (212) axis.

crystal in some other orientation would nucleate. With one configuration of heaters two solid regions developed — one at the seed crystal and the other farther up the tube. The latter would be melted at one end and would grow at the other. This second, accidental solid section frequently showed nucleation at the wall and subsequent growth of a clear single crystal. In several successive cases the orientation of this crystal was apparently the same but neither parallel nor perpendicular to the c-axis. A seed was prepared from one of these accidents and a large crystal grown from it in the usual manner. X-ray investigation showed that its direction of growth was (212) within a probable error of ± 3°. It is suggested that this may be a particularly favorable direction for growth.

Although no extensive study of quality has been carried out, samples of three crystals grown in different orientations have been compared optically and by X-ray techniques to see if quality is related to growth direction. (It has been noted by Landauer (1958, p. 3-4) and by Brill and Camp (1961, p. 3) that there seems to be a tendency for growth along the c-axis to produce a lineage structure.)

Figure 2 is a photograph of the brush figure produced when ice (uniaxial) crystals are examined between crossed Nicols in highly divergent light. In an excellent crystal, the dark lines forming the cross will be undistorted. For this picture, a crystal grown in the (212) direction was used. The detail has suffered in photography and black and white reproduction.

A more quantitative measure of the quality of a single crystal is given by the width of the reflection curves for X-ray (Bragg) reflections. Figure 3 shows curves for the (002) reflections from three different samples, one grown along the c-axis, one grown perpendicular to the c-axis and one grown along the (212) direction. It is apparent that the crystals are of good quality. However, without studying another reflection as well, one cannot assert this positively, since the (002) reflection is insensitive to rotations about the (002) direction.

Experience in growing crystals with intentionally added impurities has shown that very frequently the concentration of impurities in the ice is not uniform across the cross section of the crystal. When the tube is not rotated, convection causes different rates of circulation at different portions of the liquid-solid interface and hence different local environments.

Radial analysis of doped samples shows that the samples grown with rotation are much more uniform than those grown without rotation. However, even for a rotation rate of 6 rpm, the concentration near the wall of the tube may be about 10% greater than that at the center.

Effect of an electric field on nucleation

A series of experiments was conducted to determine whether or not the nucleation of ice crystals could be visibly affected by an applied electric field at the nucleation site. This investigation was prompted by the observation (Brill and Camp, 1961, p. 6) that the application of a potential to a condenser in which water was freezing affected the size of the crystallites formed. One hypothesis was that the field caused a migration of nuclei, possibly ions, to the electrodes at which freezing took place. Thus it might be supposed that, in a many-electrode situation where each electrode had an identical thermal environment, nucleation would occur first at those electrodes for which the electrical field condition was most satisfactory.

To examine this situation, the apparatus shown in Figure 4 was constructed. It consists of a Lucite cell with a Lucite cover which holds a set of nickel-plated brass electrodes immersed in water. The electrodes, which are rounded at the immersed end to a 1/16 in. radius, may be connected variously in pairs so as to present open-circuit, short-circuit, and potential-applied conditions as desired.

Experiments were performed using all combinations listed above under conditions of rapid freezing (ambient temperature -40C) and slow freezing (ambient temperature -10C). The applied voltage varied from zero to that at which gas evolution began (about 30 v). During nucleation and the early stages of freezing, all probes were observed simultaneously

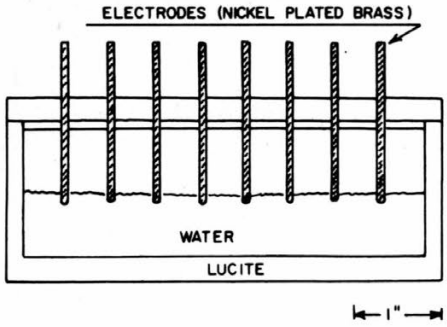

Figure 4. Apparatus to test the effect of electric fields on nucleation of ice crystals.

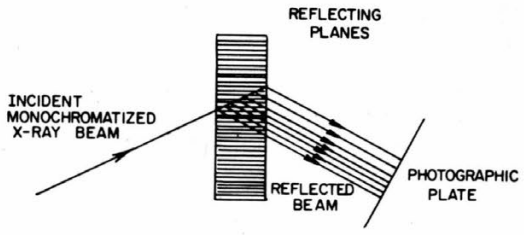

Figure 5. Illustration of the Lang technique.

by a telemicroscope. As ice formed, it seemed to grow uniformly on all probes. No preferential nucleation was observed; nor was any unusual effect at all detected.

DEGREE OF PERFECTION OF NATURAL ICE CRYSTALS

Introduction

X-ray investigations of the defect structures of ice crystals from Alaskan glaciers have shown that these crystals can be considered as having a mosaic structure (Brill and Camp, 1961, p. 13-24). This was established by comparing the experimentally measured values of the integrated intensity of X-ray reflections with those calculated from theory, assuming either perfect crystal structure or perfect mosaic structure. Measurements of the half widths of Bragg reflection peaks showed the misalignment of the mosaic blocks to be less than 3 min of arc. It has also been demonstrated that these crystals exhibit both primary and secondary extinction. These investigations have been continued using other techniques (the Lang photographic technique and the use of polarized X-rays) and by application of the refined theory of Zachariasen.

Use of the Lang technique

A technique was devised by Lang (1958, p. 597) for studying the dislocation pattern in almost perfect crystals. It can be illustrated with the aid of Figure 5. A monochromatized, parallel X-ray beam undergoes a Laue reflection. The reflected beam is photographed. For a particular position of the crystal, only a certain portion of the crystal can be examined. If, however, the crystal and the photographic film are moved together so as to scan the crystal with the beam, then the whole crystal can be examined. For a single crystal, whether perfect or mosaic, the reflected beam should be of uniform intensity. For an almost perfect crystal containing dislocations, the Lang photographs show nonuniformities. Similarly, inhomogeneities in mosaic crystals should be recorded in such photographs.

This technique has been used to examine irregularities in Alaskan ice crystals. These irregularities are slight deformations of the structure which usually cannot be detected by visual examination in polarized light. If Mo characteristic X-ray radiation (λ = 0.711 A) is used, Laue reflections of high intensities can be obtained from ice even though the crystal is quite thick (up to 1 cm). The reason for this is that the linear absorption coefficient of ice at this wavelength is small (of the order of 1). In the actual experiment the (002) reflection was photographed. The crystal and the film were stationary. Figure 6 is an example of the Lang photographs obtained from single crystal Alaskan ice. Examination of the photograph reveals the presence of irregularities in the form of streaks. These streaks are evidence of macroscopic deformations in the crystal as distinct from dislocation lines. The latter would be considerably narrower.

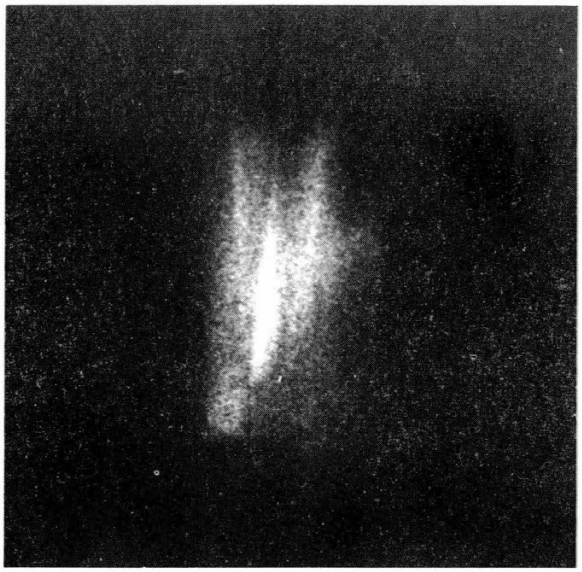

Figure 6. Lang photograph of the Laue (002) reflection from Alaskan ice crystal, 10x magnified, (.711 A X-rays). Crystal and film stationary.

Experimental tests of the mosaic crystal model of ice

Zachariasen theory. Having chosen the mosaic crystal model, one can apply an exact theoretical treatment to it. Our past work on the mosaic structure of ice has been based on the theory of Darwin as presented by James (1950). The Darwin theory assumes a mosaic structure and small mosaic blocks. The small block approximation allows a simplification to be made in calculating the integrated intensity. Results of the application of this theory are contained in Research Report 68 (Brill and Camp, 1961). A more general treatment (Zachariasen, 1946) does not assume blocks which are small and leads to somewhat different results. According to this more exact treatment, when primary and secondary extinctions are not negligible, the integrated reflecting power of a Laue reflection is given by

$$R^{\theta}_{H} = Q' \frac{T_0}{\cos\theta} e^{-(\mu_0 + g Q')\, T_0/\cos\theta} \tag{1}$$

where

$$Q' = Q\, f(A_0). \tag{2}$$

The function $f(A_0)$ depends on the size of the mosaic blocks and is given by

$$f(A_0) = \frac{\sum_{n=0} J_{2n+1}(2A_0) + |\cos 2\theta_B| \sum_{n=0} J_{2n+1}(2A_0 |\cos 2\theta_B|)}{A_0 (1 + \cos^2 2\theta_B)}, \tag{3}$$

where

$$A_0 = \frac{e^2}{mc^2} \frac{|F|}{V} \lambda \frac{t_0}{\cos\theta}. \tag{4}$$

The meaning of the different symbols is as follows:

T_0	is the thickness of the crystal plate
θ_B	is the Bragg angle
θ	is the angle between the normal to the crystal plate and the incident X-ray beam
μ_0	is the linear absorption coefficient
g	is called the coefficient of secondary extinction (and is determined from the effective absorption coefficient by the relation $\mu' = \mu_0 + gQ'$)
J	is the Bessel function
e^2/mc^2	is the classical radius of the electron
F	is the geometrical structure factor
V	is the volume of the unit cell
t_0	is the thickness of the mosaic block
λ	is the X-ray wavelength used

$$Q = \left(\frac{e^2}{mc^2}\right)^2 \frac{F^2}{V^2} \frac{1 + \cos^2 2\theta_B}{2 \sin 2\theta_B}. \tag{5}$$

Equation 1 is the basis for determination of the sizes of the mosaic blocks. If $\underline{R}^{\theta}_{H}$ is determined experimentally for several thicknesses, $\underline{T}_0$, of the crystal plate, and $\ln(R^{\theta}_{H} \cos\theta/T_0)$ is plotted vs $T_0/\cos\theta$, then the ordinate corresponding to $T_0 = 0$ gives the value of Q'. Having determined Q' experimentally, the value $\underline{f}(\underline{A}_0)$ can be calculated from eq 2. Relations 3 and 4 can then be used to determine the thickness $\underline{t}_0$. Obviously eq 3 is in general unwieldy. However, for values $\underline{A}_0$ which are not too large (of the order of 1), the Bessel functions $J_{2n+1}(2A_0)$ can be expressed in terms of a series which will converge reasonably quickly. If we use the series (Vand, 1953)

$$\sum_{n=0} J_{2n+1}(2x) = x - \frac{x^3}{3} + \frac{x^5}{20} - \ldots \pm \frac{x^{2n+1}}{(2n+1)(n!)^2} \tag{6}$$

then the function $\underline{f}(\underline{A}_0)$ is given by

$$f(A_0) = 1 - \frac{1}{3} A_0^2 \frac{1 + \cos^4 2\theta}{1 + \cos^2 2\theta} + \frac{1}{20} A_0^4 \frac{1 + \cos^6 2\theta}{1 + \cos^2 2\theta} - \frac{1}{252} A_0^6 \frac{1 + \cos^8 2\theta}{1 + \cos^2 2\theta} + \tag{7}$$

If the cosine factors do not vary excessively, which will be the case for small angles, then either the mean of all factors can be used, or all of them can be equated to the first one. In the latter case

$$f(A_0) = 1 - \frac{1 + \cos^4 2\theta}{1 + \cos^2 2\theta} \left[\frac{1}{3} A_0^2 - \frac{1}{20} A_0^4 + \frac{1}{252} A_0^6 - \frac{1}{5,184} A_0^8 + \ldots\right]. \tag{8}$$

This relation has been used to re-evaluate the thicknesses of the mosaic blocks from the data given in Research Report 68 for Mo characteristic X-ray radiation. These data are reproduced in Table I for reference.

Table I

Order	Q'	Q	$f(A_0)$
(002)	1.10×10^{3}	3.82×10^{3}	.283
(002)	1.6×10^{3}		.277
($\bar{1}$10)	7.5×10^{4}	1.82×10^{3}	.413

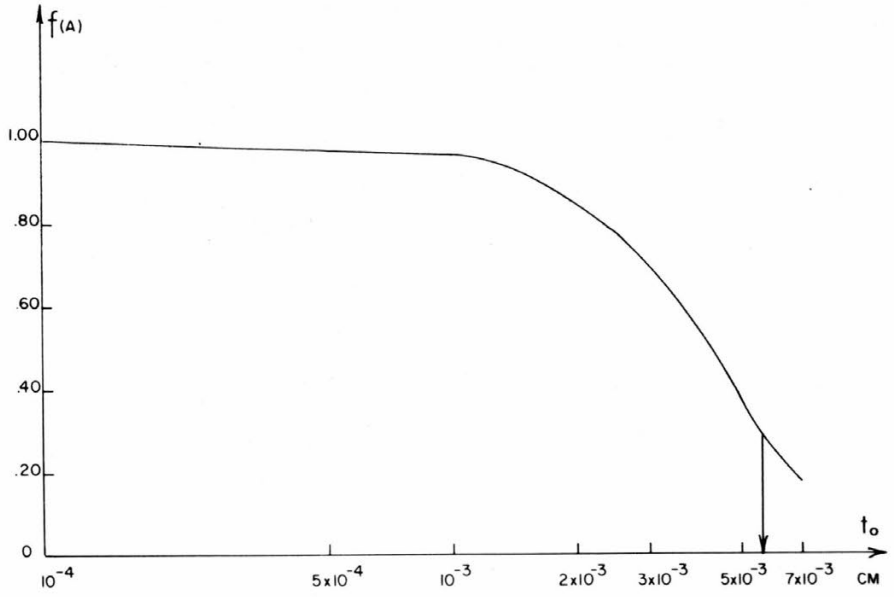

Figure 7. $f(A_0)$ vs t_0 for (002) reflection from ice.

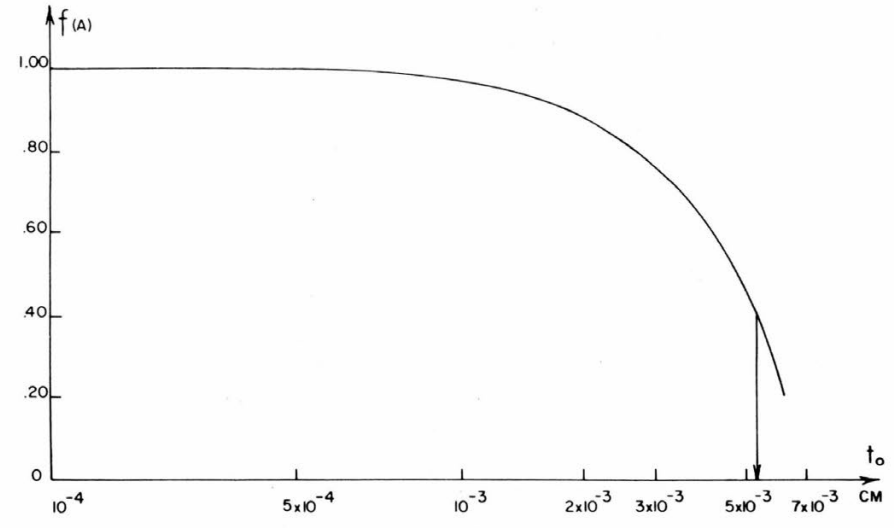

Figure 8. $f(A_0)$ vs t_0 for ($\bar{1}$10) reflection from ice.

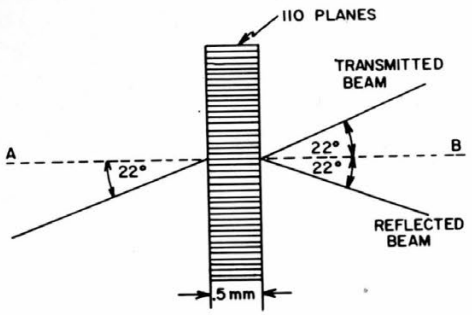

Figure 9. Illustration of the Borrmann effect.

The plots of $\underline{R}_H^{\theta}$ vs $T_0/\cos\theta$ for the actual experimental data are contained in Research Report 68.

In order to obtain the values of $\underline{t}_0$, the function $\underline{f}(A_0)$ has been plotted vs $\underline{t}_0$ for the (002) and (110) reflections for Mo X-ray radiation (Fig. 7, 8). Equation 8 has been used for this purpose. From these graphs and the results from Table I we find $t_0 = 5 \times 10^{-3}$ cm for both reflection orders instead of the previously obtained values of $t_0 = 10^{-3}$ cm. Thus this is the characteristic dimension of the mosaic blocks as seen by Mo X-ray radiation.

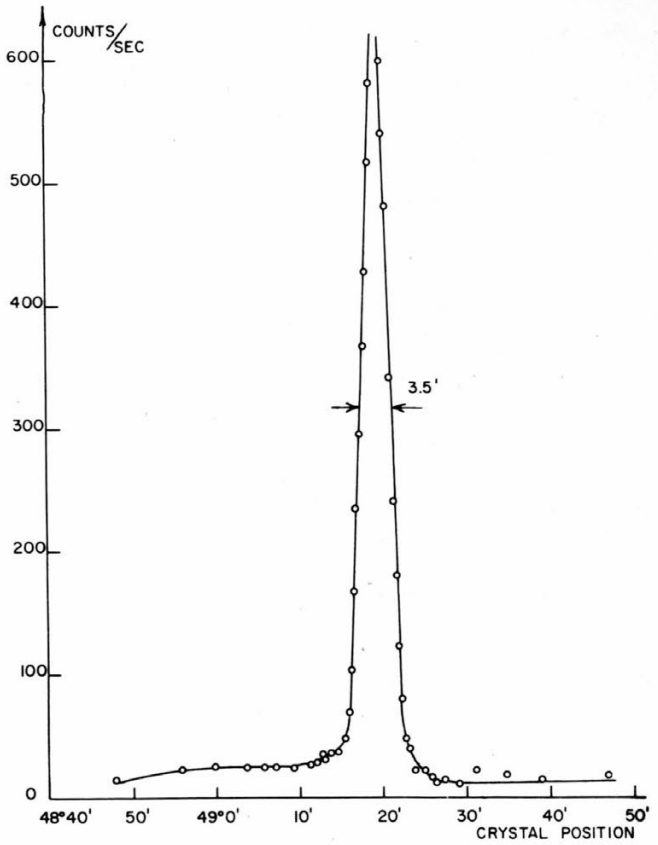

Figure 10. An (002) reflection curve from ice.

Half-width of the reflection curve. Some results of the study of half-widths of X-ray reflection curves have already been reported in Research Report 68. In those experiments the incident X-ray beam was monochromatized by an NaCl crystal. Recently, we have been able to improve the monochromatization through the use of the Borrmann effect. By the use of this effect the incident X-ray beam also was made less divergent.

In 1941 Borrmann (1941, p. 147) discovered a mechanism for anomalous transmission of X-rays through nearly perfect crystals. The effect may be described with the aid of Figure 9 which illustrates our experiments. Intense CuKα X radiation (18 μ at 30 K) is incident upon a germanium crystal plate cut so that the (110) planes are perpendicular to the large surfaces of the crystal. Ordinarily, no radiation is observed to pass through the crystal. However, if the incident beam makes an angle of 22° (the Bragg angle) with the (110) planes, two beams emerge on the other side of the crystal: one, referred to in the figure as the transmitted beam, goes in the direction of the incident beam, and the other, called the reflected beam, goes in the direction predicted by Bragg's law.

In our experiments, the Ge crystal was placed near the window of the X-ray tube and the two beams obtained. The reflected beam was used as the incident beam for the X-ray reflection from ice. Figure 10 is an intensity curve for the (002) reflection from an Alaskan ice crystal. The half-width is about 3.5 min of arc in conformity with our previous results. Most of this width may now be assigned to the imperfections in the ice crystal itself.

Investigations with polarized X-rays. An X-ray beam leaving the X-ray tube is unpolarized. The integrated surface reflections of such a beam from an ideal mosaic and from a perfect non-absorbing crystal are given respectively by

$$\rho_m = R_m (1 + \cos^2 2\theta_B) \tag{9}$$

and

$$\rho_p = R_p (1 + |\cos 2\theta_B|), \tag{10}$$

where

$$R_m = \frac{1}{2\mu_0} \frac{\lambda^3}{V^2} |F|^2 \left(\frac{e^2}{mc^2}\right)^2 \frac{1}{2 \sin 2\theta_B} \tag{11}$$

and

$$R_p = \frac{8}{3\pi} \frac{\lambda^2}{V} |F| \frac{e^2}{mc^2} \frac{1}{2 \sin 2\theta_B}. \tag{12}$$

If the incident X-ray beam is completely polarized and the electric vector makes an angle ϕ with the plane of reflection, the integrated reflections in the two respective cases are (Ramaseshan and Ramachandran, 1953, p. 364)

$$\rho_M(\phi) = R_M(\cos^2 \phi + \sin^2 \phi \cos^2 2\theta_B) \tag{13}$$

$$\rho_p(\phi) = R_p(\cos^2 \phi + \sin^2 \phi |\cos 2\theta_B|). \tag{14}$$

Let $\rho_M(o)$ and $\rho_p(o)$ be the values of the integrated reflections when $\phi = 0$. Then the ratios

$$r_M(\phi) = \frac{\rho_M(\phi)}{\rho_M(o)}$$

$$r_p(\phi) = \frac{\rho_p(\phi)}{\rho_p(o)},$$

are given respectively by

$$r_M(\phi) = \cos^2 \phi + \sin^2 \phi \cos^2 2\theta_B \tag{15}$$

and

$$r_p(\phi) = \cos^2 \phi + \sin^2 \phi |\cos^2 \theta_B|. \tag{16}$$

Except for special values of θ_B, the two functions $r_M(\phi)$ and $r_p(\phi)$ are different. The fact that these functions can be made quite different for a reasonable choice of θ_B supplies us with what seems to be a rather simple test of investigating different crystals. The experimental procedure is to render the incident X-ray beam completely polarized and to obtain an experimental curve $r(\phi)$ versus ϕ. This curve is then compared with the theoretical curves for $r_M(\phi)$ and $r_p(\phi)$.

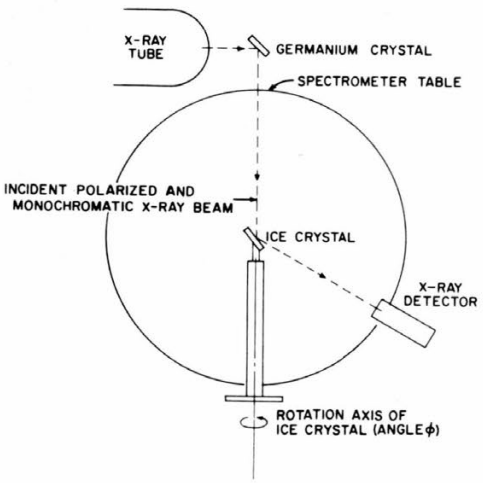

Figure 11. Experimental arrangement for investigating the dependence of reflection of polarized X-rays on the degree of perfection of crystals.

To obtain a completely polarized incident X-ray beam, the Bragg angle of the monochromator has to be 45° or close to it. The (333) reflection of Cu X-rays (1.54 A) from a germanium crystal occurs at an angle differing by only a few minuted of arc from 45°. This reflection was used to obtain a completely polarized X-ray beam.

In order to investigate the variations of the reflected intensities with the angle ϕ, the axis of the crystal-carrying arm of the spectrometer was aligned with the incident X-ray beam. The crystal holder was then rotated about the incident beam. In this way the angle ϕ could be varied from 0° to 90° (or more). Of course, the beam reflected from the ice crystal was no longer in the horizontal plane of the spectrometer. This necessitated construction of a special arc on which the counter could be moved to receive the reflected beam. Figure 11 shows the experimental arrangement used.

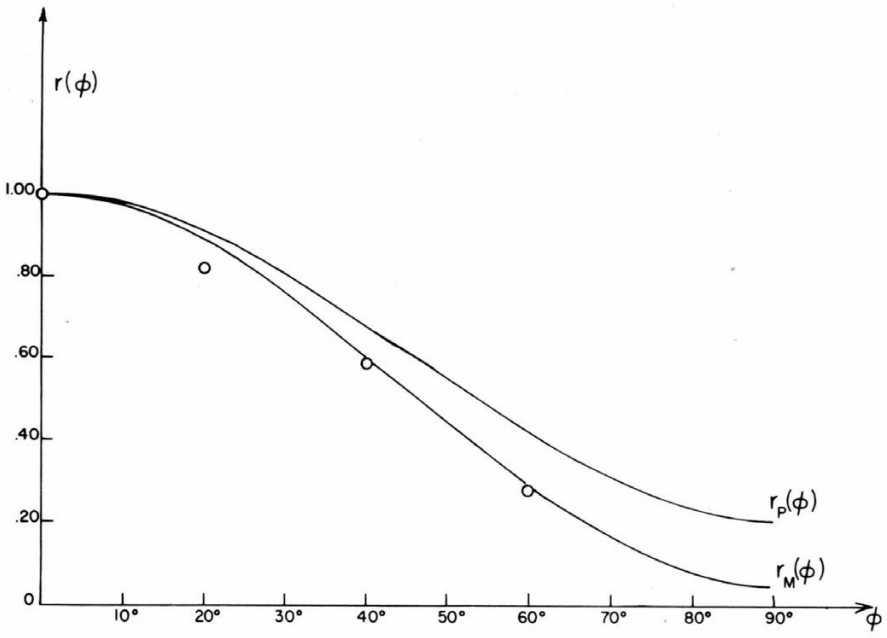

Figure 12. Theoretical curves (solid lines) and the results of experiments (points) on the dependence of reflected intensities of polarized X-rays on the degree of perfection of crystals. (006) reflection from ice. 1.54 A X-rays.

The (006) reflection from ice was studied and the results are shown in Figure 12. The two solid curves $r_P(\phi)$ and $r_M(\phi)$ are respectively the theoretical curves for a perfect crystal and for a perfect mosaic crystal. The points are the experimental data and confirm the mosaic character of the Alaskan ice crystal. It may be emphasized that, apart from the normalization, no adjustable parameters were involved in plotting the experimental points.

In summary, the degree of perfection of Alaskan ice crystals has been examined by three methods. The polarization method established in a qualitative way that the ice crystals may be regarded as mosaic. Measurements of the half-width of reflection curves showed that the angular spread of mosaic blocks is not large. The value obtained for the Alaskan ice is about 3 min of arc. This should be compared with one or more degrees of arc exhibited by some mosaic crystals.

Application of Zachariasen's theory to the mosaic crystal model yielded a value for the angular spread of the mosaic blocks of about 1 min of arc and a characteristic dimension of the mosaic blocks of about 5×10^{-3} cm.

THERMAL PROPERTIES OF THE ICE LATTICE

Thermal motion of ice molecules

The problem of thermal motion in ice crystals has been studied extensively in the past (Brill, 1957, p. 54-65; Brill and Camp, 1961, p. 25-40; Zajac, 1958, p. 1324). However, all the previous work has been concerned with the amplitude of the oxygen motion or of the hydrogen motion in the direction of the c-axis. In order to have a complete picture of the vibrational motion in ice, it is necessary to determine also the amplitude of the motion in a direction perpendicular to the c-axis.

Theory shows (James, 1950) that different X-ray reflections are particularly suited to measuring components of vibration in given directions. For example, (00ℓ) type reflections give information only about motion parallel to the c-axis. The (πxo) reflections exclude all motion parallel to the c-axis. For this reason, we have studied the temperature behavior of the $(\bar{2}20)$ and $(\bar{3}30)$ reflections for single crystals of Alaskan glacier ice. The incident X-ray beam was the Mo characteristic X-ray radiation of 0.711 A wavelength. The experiments consisted of determining the total number of counts, $E_{(\bar{2}20)}$ and $E_{(\bar{3}30)}$, as the ice crystal was rotated with the same angular velocity through the Bragg angle for each of the two reflections. These numbers correspond to the total reflected X-ray energies in the two cases. Both measurements were made at the same absolute temperature T. Using these experimental data, the Debye characteristic temperature, θ_D, can be determined from the relation (Brill and Camp, 1961, p. 25-40)

$$m\,\theta_D^2 = \frac{12\,h^2}{k\lambda^2}\;T\;\frac{\Delta(\sin^2\theta_B)}{\ln(J_1/J_2)}. \qquad (17)$$

In this expression, m is the mass of the H_2O molecule, h is Planck's constant, k is Boltzmann's constant,

$$\Delta(\sin^2\theta_B) = \sin^2\theta_{\bar{3}30} - \sin^2\theta_{\bar{2}20},$$

and

$$J = \frac{E}{|F|^2\,W},$$

in which F is the geometrical structure factor and W is the polarization factor. In order to employ this method, the geometrical structure factors $F_{(\bar{2}20)}$ and $F_{(\bar{3}30)}$ had to be evaluated.

Two series of experiments were performed at temperatures 267 and 239K and two Debye characteristic temperatures were obtained. The mean value of these is θ_D = 226K. This value may be compared with the Debye characteristic temperature obtained previously from the intensities of the (00ℓ) type of reflections. The value of the latter is θ_D = 224 ± 8K. Thus the newly determined Debye temperature lies within the experimental error of the one determined previously.

The amplitude of the thermal motion can be expressed directly in terms of the Debye characteristic temperature. Our present results seem to point to the conclusion that the molecular vibrations in ice are nearly isotropic.

Temperature dependence of the lattice parameters of ice

The lattice parameters, a and c, of ice have been measured by several different people in different laboratories and at different temperatures. Lonsdale (1958, p. 424) has compiled these results and from the composite has estimated the variation with temperature. However, the scatter of experimental data is great and only a few points cover a large temperature region. This fact has prompted us to make a careful study of the temperature dependence of the lattice parameters c and a for large single crystals of ice. Recently LaPlaca and Post (1960, p. 503-505) made a similar series of measurements on tiny ice crystals deposited from the vapor phase onto glass plates.

Our experimental procedure was to measure the temperature dependence of the Bragg angle and then obtain the value of d, the spacing between the reflecting planes, from the Bragg relation

$$2\,d \sin\theta_B = n\lambda.$$

For the (00ℓ) type reflection, Bragg's law becomes $2\,c \sin\theta_B = n\lambda$, giving c directly. Similarly, for ($\bar{h}$ho) reflection, Bragg's law becomes $2\frac{a}{2} \sin\theta_B = n\lambda$ giving a directly. These two types of reflections were used in our work.

The greatest sensitivity to variations in a and c will occur for the largest order, n, measurable. With CuKα radiation of 1.54 A wavelength, the greatest value of n is 8 for the (00ℓ) type of reflection and 2 for the ($\bar{h}$ho) type. Thus the two reflections (008) and ($\bar{2}$20) were employed.

To obtain the temperature dependence of the Bragg angle θ_B, reflection curves were traced out at various temperatures. The shift of the peak could be read on the chart and the corresponding change of the Bragg angle evaluated.

Our experimental arrangement gives accurate values only of the change in θ_B. However, in other experiments (Brill and Camp, 1961, p. 8-12) the values of θ_B have been accurately determined at one temperature by the back reflection powder technique. From this work the values of a and c were calculated and found to be

$$a = 4.511 \pm 0.001 \text{ A}$$
$$c = 7.345 \pm 0.001 \text{ A}$$

both at temperature -40.5C. Using these values and our measurements, the absolute magnitudes of the a and c parameters could be calculated for the various temperatures.

Several experiments have been performed to determine the temperature variation of the a and c parameters of ice for Alaskan ice crystals. The results are shown in Figures 13 and 14. The curve for the c-axis (Fig. 13) is the result of two sets of measurements and the curve for the a-axis (Fig. 14) is a plot for three sets of measurements.

It can be seen that the scatter of experimental points is considerable (but very much smaller than in Lonsdale's compilation). In order to discuss the possible sources of error, it will be well to describe our experimental arrangement. Large single crystals of ice ($\frac{1}{2}$ x $\frac{1}{2}$ x $\frac{1}{4}$ in.) were mounted in a housing which was fastened to a goniometer head

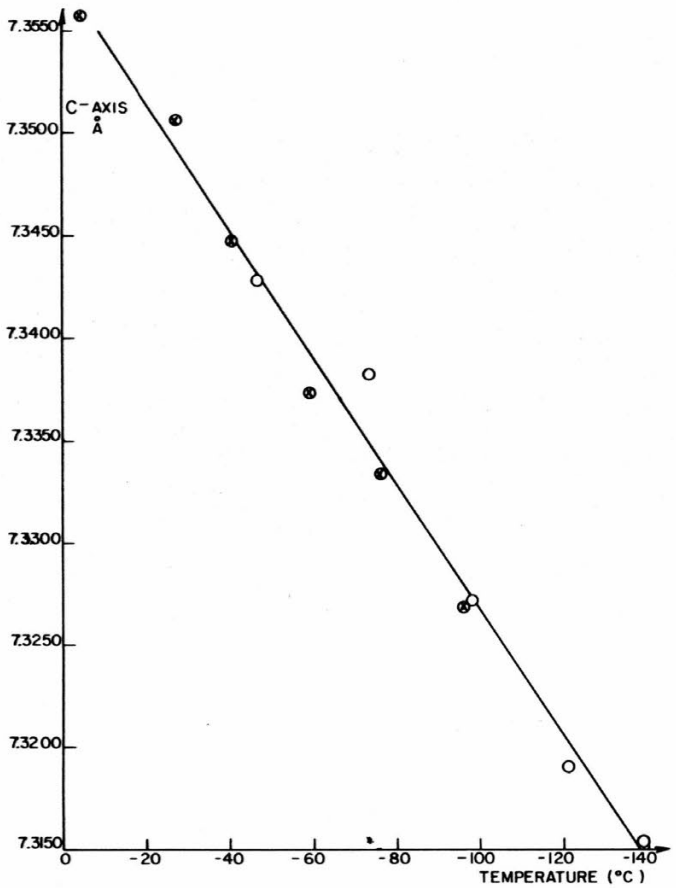

Figure 13. Temperature dependence of the c parameter of ice.

(placed in a horizontal position). The goniometer head was mounted on the crystal-carrying arm of the spectrometer table. By rotating this arm, the Bragg reflection of X-rays was obtained.

The sample was cooled by liquid nitrogen vapor. As the temperature was lowered, the housing, goniometer head, and crystal-carrying arm became cold and some warping of these mountings may have occurred, resulting in errors in the angle θ_B.

In order to estimate how extensive such warping may be, the ice crystal was replaced by a mirror and the incident X-ray beam by a beam of light. The apparatus was then cooled in the usual manner and the changes in the angle of the mirror were measured. The results are shown in Figure 15. The maximum overall change in mirror angle was about 0.3 min of arc. Although this experiment does not tell us specifically about movement of the arm or displacement of the crystal, it does indicate that mechanical distortions of the apparatus due to temperature change are very small.

The large scatter in the experimental points of Figures 13 and 14 is attributed to the errors resulting from the initial setting of the crystal-carrying arm before the reflection curve was traced out. This initial setting had an error of about 1 min of arc associated with it.

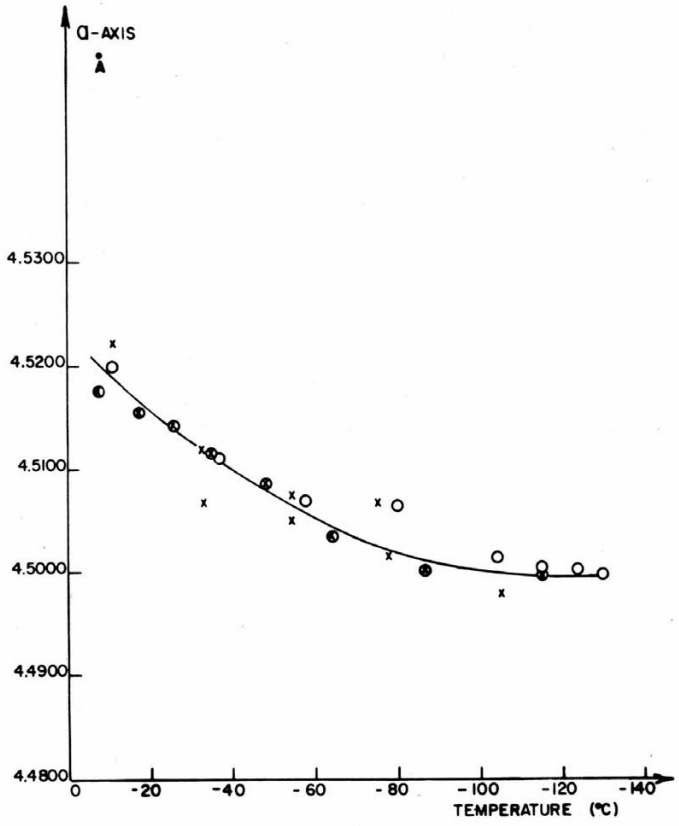

Figure 14. Temperature dependence of the a parameter of ice.

Measurement of the coefficient of thermal expansion of bulk single-crystal ice

In the next section, the temperature dependence of the lattice parameters of ice is discussed. Interesting conclusions in regard to the structure of ice can be drawn from a comparison of the behavior of the bulk coefficients of expansion with those of the lattice parameters. These bulk coefficients have been measured by several workers. Jakob and Erk (1928, p. 125) used micrometer methods in a careful series of measurements on polycrystalline ice over the temperature range -250C to 0C. Single-crystal measurements have been performed also (Powell, 1958, p. 464-466), but fairly large discrepancies exist among the published values; in particular, there seems to be a real difference between these values and those for the coefficients of expansion of the lattice parameters as measured by X-rays. Thus an apparatus has been designed which is intended to measure the coefficients for bulk single-crystal ice.

In order to make accurate measurements of the expansion coefficient, we must first measure the length of a sample with precision, then accurately measure the change in temperature and the change in length. In order to measure the temperature accurately, the sample must be short so that it will be of uniform temperature; this fact makes the other two measurements more difficult. It is believed that these problems can be resolved by using a multiple beam interferometric technique to measure very small changes in length.

The rudiments of our original apparatus are shown in Figure 16. The ice sample S rests on an Invar platform B suspended in a Dewar beaker by Invar rods, R, from a

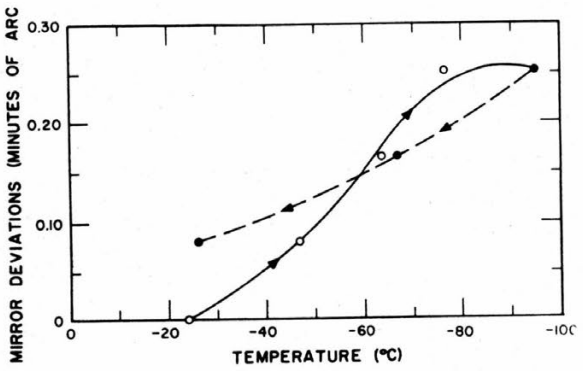

Figure 15. Deflection of mirror vs temperature.

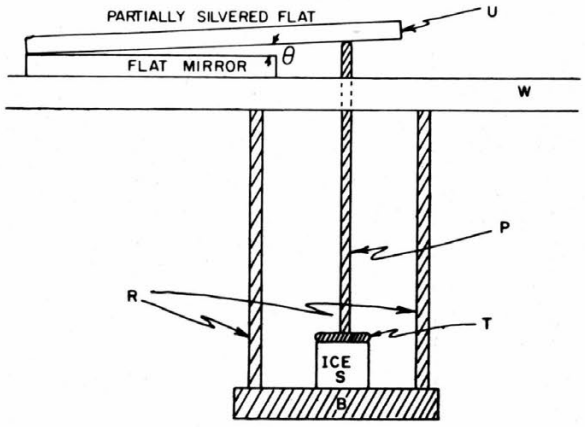

Figure 16. Apparatus for measurement of thermal expansion as first designed.

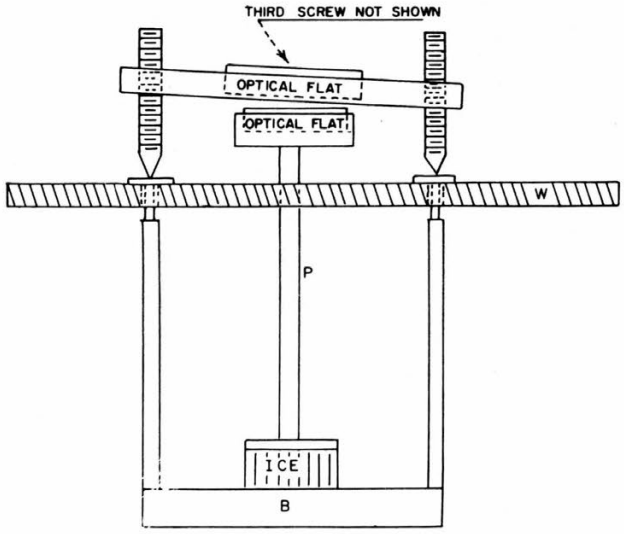

Figure 17. Modified arrangement for thermal expansion measurement.

brass plate, W. An Invar rod, P, supported by an Invar plate, T, which rests on top of the sample, extends through a loose bushing in W to transmit changes in sample length to an optical wedge, U, outside of the beaker. As the temperature inside the beaker is changed, the wedge opens or closes and fringes move past a fiducial mark accordingly. The wedge and optical system are of standard design. In complete detail, the apparatus is somewhat more complicated than shown in Figure 16. It requires porcelain sections of equal length in each of the members R and P to reduce the flow of heat into the beaker and an arrangement of baffles to provide uniform temperature throughout the sample. The sample temperature is measured by means of a thermocouple embedded in it.

A series of measurements on ice and other materials has convinced us that there are systematic errors of the order of 5% introduced by our apparatus. After considerable study, we have concluded that much of this error is due to the effect of changing room temperature on the portion of the system above the plate W. To eliminate this source of

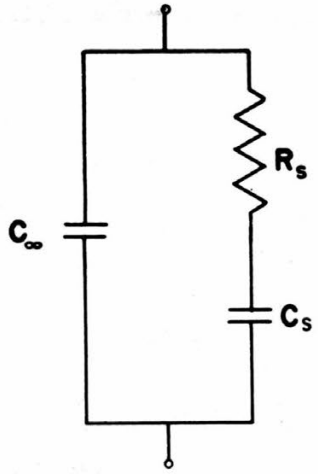

Figure 18. Electrical equivalent of a pure Debye relaxation.

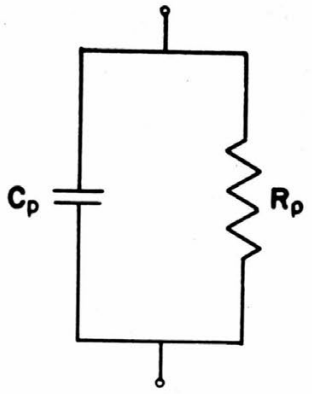

Figure 19. Parallel equivalent for Figure 18. Parameters are functions of frequency.

error, major changes have been made in the mounting for the optical system as shown in Figure 17. The whole apparatus is hung from the top of plate W, thus eliminating any effect due to its expansion or contraction. Moreover all elements except the mirror above the plate W are constructed of Invar. The mirrors themselves are made of fused quartz and supported in such a way as to minimize strains and bending. This apparatus will be ready for test shortly.

DIELECTRIC PROPERTIES OF ICE

Dielectric properties of ice crystals containing very low concentrations of NH_4F

Measurements have been continued of the audiofrequency dielectric relaxation of pure and NH_4F-contaminated ice. Extensive measurements of this kind were reported in earlier reports (Brill, 1957; Brill and Camp, 1961). The principle contributions of the recent work have been in the use of single crystal samples, the extension of the measurements to the region of very low concentration, and in experiments to determine whether the phenomena observed are independent of the length of the sample. In addition some improvements have been made in technique.

The preparation of the single crystal samples has been covered earlier. From the experience gained in these activities, it should be emphasized that, unless care is taken to avoid it, the concentration of impurity will not be uniform throughout the sample. Thus any data reported for doped polycrystalline samples must be regarded with some suspicion.

If the relaxation process is governed by an activation energy ϵ, the frequency at which the maximum power per cycle is dissipated in the sample, f_m, will be related to temperature by an expression of the form

$$1/\tau = 2\pi f_m = k\, e^{-\epsilon/RT}$$

in which k is some constant. If the process can be represented by a simple Debye dispersion, it has an electrical analogue shown in Figure 18.

At any particular frequency ω, this circuit has an electrical equivalent given by Figure 19. The two are related by eq 18a, b and 19a, b

$$R_s = \frac{R_p}{1 + \omega^2 R_p^2 C_p^2} \qquad (18a)$$

$$C_s = \frac{1 + \omega^2 R_p^2 C_p^2}{\omega^2 R_p^2 C_p} \tag{18b}$$

$$R_p = \frac{1 + R_s^2 C_s^2 \omega^2}{R_s C_s^2 \omega^2} \tag{19a}$$

$$C_p - C_\infty = \frac{C_s}{1 + R_s^2 C_s^2 \omega^2} = \frac{C_s}{1 + \omega^2 \tau^2} \tag{19b}$$

where

$$\tau = R_s C_s = \frac{1}{\omega^2 R_p C_p} = \frac{1}{2\pi f_m} .$$

A plot of $1/\omega R_p$ vs C_p for different values of ω yields a semicircle of radius $C_s/2$ whose origin is at the point $C_p = C_s/2 + C_\infty$ and $1/\omega R_p = 0$. This fact is of considerable use, for it provides both a test for a Debye dispersion and a means of analysis which brings together data of all frequencies. The frequency at which $1/\omega R_p$ is a maximum is f_m. Since some parallel capacitance due to leads, etc. is unavoidable and must be subtracted, it is more convenient to measure R_p and C_p directly than it is to measure R_s and C_s. The values of R_s and C_s can then be obtained from eq 18 and 19. The technique of plotting $1/\omega R_p$ against C_p was first applied to ice by Cole and Cole (1941, p. 341-351) and such a graph is now frequently referred to in the literature as a "Cole plot".

If there is more than one process present, the situation is more difficult to analyze. Figure 20 shows the equivalent circuit and the construction of the resultant Cole diagram for the case of two Debye dispersions. It is evident from the construction that the resultant is still nearly a circle whose center has been moved toward larger C_p by an amount $C_2/2$ and has been depressed by an amount nearly equal to $1/\omega_1 r_1 + 1/\omega_2 r_2 - 1/\omega_m r$ where ω_1 is $2\pi f_{m1}$, $\omega_2 = 2\pi f_{m2}$, $\omega_m = 2\pi f_m$, and f_m is the frequency at which the composite curve reaches its largest value of $1/\omega R_p$. It is significant that the data for pure ice generally lead to Cole plots for which the center is close to the C_p axis, while the data for ice containing a trace of NH_4F invariably require a center well below the C_p axis.

Much experimental data obtained in this way for polycrystalline samples containing in excess of 0.01% NH_4F by weight has been published in earlier reports (Brill, 1957; Brill and Camp, 1961). But the results for lower concentrations have been inconclusive. This range has now been investigated using single crystal samples grown in the direction of the c-axis and measured with the field applied along the c-axis. The lowest concentration used was 0.00035%. Analysis of the data leads to a linear relation between log τ and $1000/T°K$ which indicates a normal Debye type dispersion and an activation energy of about 13 kcal/mole which is characteristic of pure ice. The measurements were carried to a temperature of -42C and it seems clear from later work that an impurity effect would have been observed had the experiments been carried to a sufficiently low temperature.

The results for three samples of concentration 0.0025%, 0.0031% and 0.0042% respectively are shown in Figure 21. In each case the high temperature portion of the curve resembles that for pure ice. However, at a sufficiently low temperature the data become asymptotic to another line characteristic of a very much smaller activation energy. These curves can be analyzed as sums of exponentials

$$1/\tau = k_1 e^{-\epsilon_1/kT} + k_2 e^{-\epsilon_2/kT}$$

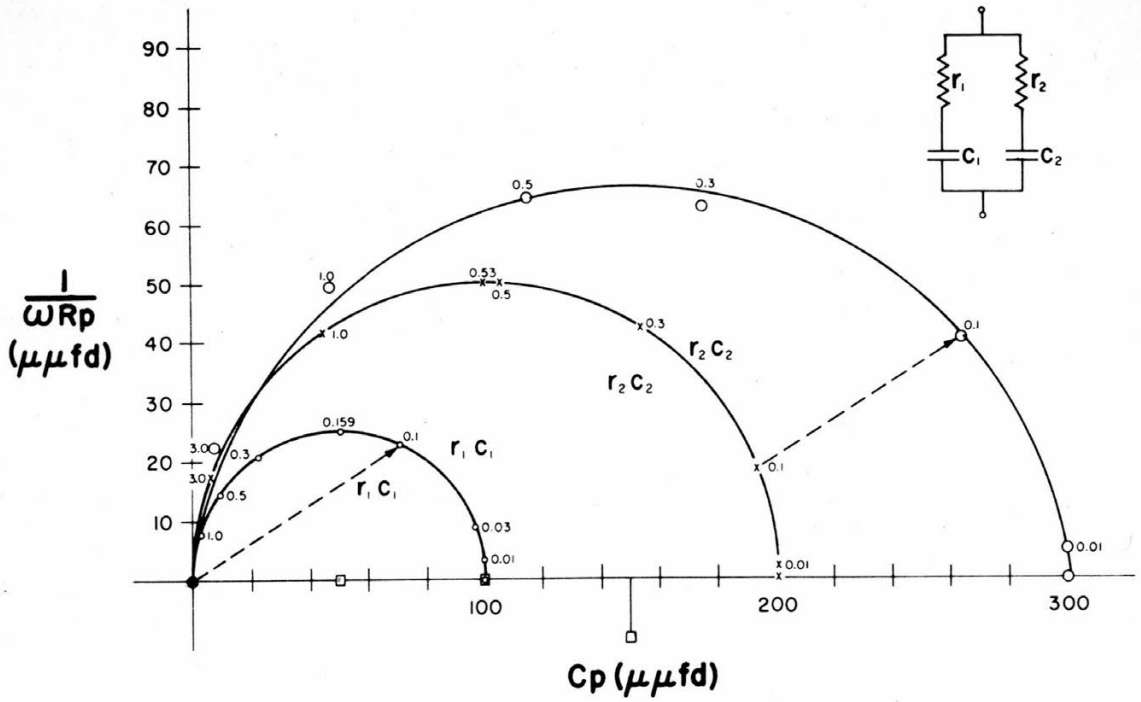

Figure 20. Cole diagrams for two arbitrary Debye relaxations and the Cole diagram for the two in parallel, constructed by adding the vector from the origin to a given point on one to the vector to the corresponding point on the other. Center of the compound diagram is square box below the c' axis.

yielding a common ϵ_1 = 13.5 ± 1 kcal/mole for the first slope. Because of the limited temperature range over which the experiments were conducted, it is not clear whether or not the second slopes are common also. However, within the limit of experimental error a common ϵ_2 of 0.6 ± 0.4 kcal/mole may be assigned.

Recently a theoretical treatment of dielectric relaxation and conductivity in ice has been published by Granicher et al. (1957, p. 50-62). A central thesis of this theory is that orientational, or Bjerrum, defects are present in the crystal in a number which depends on the temperature, the activation energy for their formation, and the impurities present. These defects are caused thermally by the rotation of water molecules to produce doubly occupied bonds and vacant bonds in defiance of the Bernal-Fowler rules. Bjerrum defects are constantly being generated and recombining so that at any temperature an equilibrium number will be wandering through the lattice. Any molecule adjacent to such a defect is in a much more favorable situation for rotating than is a normal molecule. As a result, when an external field is applied to a crystal, it is only those molecules which adjoin Bjerrum defects which are influenced. As the defects move around, they eventually contact all the molecules and equilibrium in the field is established. The relatively long dielectric relaxation time for ice thus reflects the time it takes for these defects to make contact with most of the molecules. Since one type of defect may create a more favorable situation for molecular rotation than the other, it is reasonable to expect one of them to be dominant. Granicher concluded that the doubly occupied bond (D defect) creates a more favorable situation for rotation than the vacant bond (L defect) and that consequently the activation energy for dipole rotation in pure ice is

$$E_0/2 + E_{rot}^{(D)} = 13.15 \text{ kcal/mole.}$$

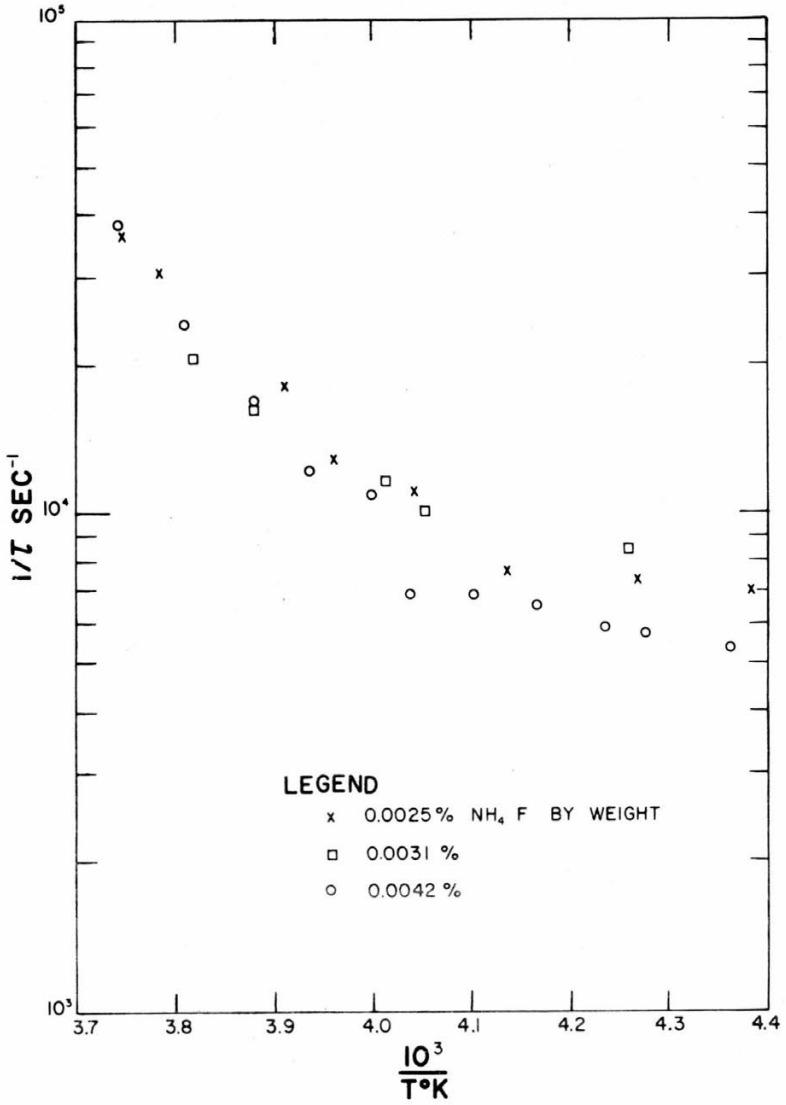

Figure 21. Semi-log plot of $1/\tau$ vs $1000/T°K$ for samples containing 0.0025%, 0.0031% and 0.0042% by weight of NH_4F.

in which $\underline{E}_{rot}^{(D)}$ is the energy required to rotate a molecule in the presence of a $\underline{D}$ defect and $\underline{E}_0$ is the energy of formation of a Bjerrum defect pair. He finds the value

$$21.9 < E_0 < 26.2 \text{ kcal/mole and}$$

$$E_{rot}^{D} < .46 \text{ kcal/mole.}$$

The addition of foreign atoms as substitutional impurities may increase the concentration of one or the other type of defect or leave it unchanged. In the latter event, as in the case of interstitial impurities, only those molecules in the immediate neighborhood of the impurity site will be affected. Although the local dielectric properties may be disturbed, the contribution of this to the total will be small for concentrations below a few percent. It appears that a trace impurity can profoundly affect the dielectric properties of the whole only when the impurity can act as a generator of Bjerrum defects

and thereby change the equilibrium number of these defects throughout the lattice. The situation is very similar that of a semiconductor (or insulator) to which donor or acceptor atoms have been added.

The case in which an impurity atom creates L and D defects in equal numbers is an interesting one. It is analogous to adding equal numbers of donor and acceptor impurities to an intrinsic semiconductor (Kittel, 1956, p. 359). The equilibrium number of L and D defects in this case will be independent of impurity concentration provided that the ionization energies of these defects are equal. By energy of "ionization" we mean the energy required to cause an adjacent molecule to rotate in such a way as to move the defect away from the impurity site.

If the activation energies for ionization of the impurity sites are not equal, the situation becomes very complex. Simplification may be found in the extreme cases in which the ionization energy for one type is much larger than that for the other. In this case the behavior of the system is expected to be similar to that in which the system is doped only with impurities having the lower ionization energy. In the case of NH_4F as a substitutional impurity, the molecular structure suggests that equal numbers of L and D defects are created, if indeed any are created at all.

The introduction of NH_4F as a substitutional impurity in the lattice may alter the dielectric properties in two ways. It may create an excess of one or the other type of Bjerrum defects or it may create local regions in the immediate vicinity of the impurity atom at which dipole rotation becomes enhanced. In the first case, we would expect a decrease in relaxation time due to the increased number of defects but little change in the d-c dielectric constant or in the shape of the dispersion curve. For temperatures so low that the impurity-created defects are much more abundant than those created thermally, the relaxation time would be governed by the activation energy for defect ionizations. For sufficiently high temperatures, the thermally-created defects will outnumber the impurity-created defects and the behavior will be similar to that for pure ice. The temperature at which the transition from one case to the other takes place will depend on impurity concentration, increasing as the concentration increases.

In the second case, the ease of dipole rotation is altered only in the immediate vicinity of the impurity ions. Thus for low concentrations of NH_4F, the dielectric constant associated with these regions should be added to the dielectric constant of the whole. The result would be a double humped dispersion curve and an increase in the extrapolated d-c value of the dielectric constant. Figure 22a is a plot of the frequency dependence of c' (proportional to the dielectric constant) for a sample doped with 0.0025% NH_4F by weight. As seen in Figure 21, a transition from pure to doped behavior occurs in the region of $\frac{10^3}{T} = 4.1$ or T = 244K. Figure 22a shows that no significant change occurs in the shape of the dispersion curve in this temperature region. Figure 22b, a plot of the extrapolated d-c dielectric constant as a function of 1000/T, for three different concentrations of NH_4F shows no trend in regard to concentration. The sample thickness was difficult to control accurately in these experiments and the apparent difference in dielectric constant from sample to sample may well be experimental error. However, it remains clear from Figures 22a and 22b that local disturbance about the impurity ions is not an important factor in the experimental results. Thus we conclude that NH_4F introduces Bjerrum defects with an excess of one type or the other.

Assuming that the knees of the curves in Figure 21 occur at a temperature for which the excess of one type of defect is equal to the number created thermally, it is possible to calculate the effectiveness of NH_4F in producing defects. For a concentration of 0.004%, the knee occurs at about -25C. Granicher computes the number of thermally excited Bjerrum defects at this temperature to be between 10^{13} and 5×10^{14} per cm^3. It follows that only about one net unbalanced defect occurs for each thousand NH_4F molecules. An unbalance of this magnitude can easily be accounted for in terms of the theoretical approximations which have been used (e.g., equal ionization energies).

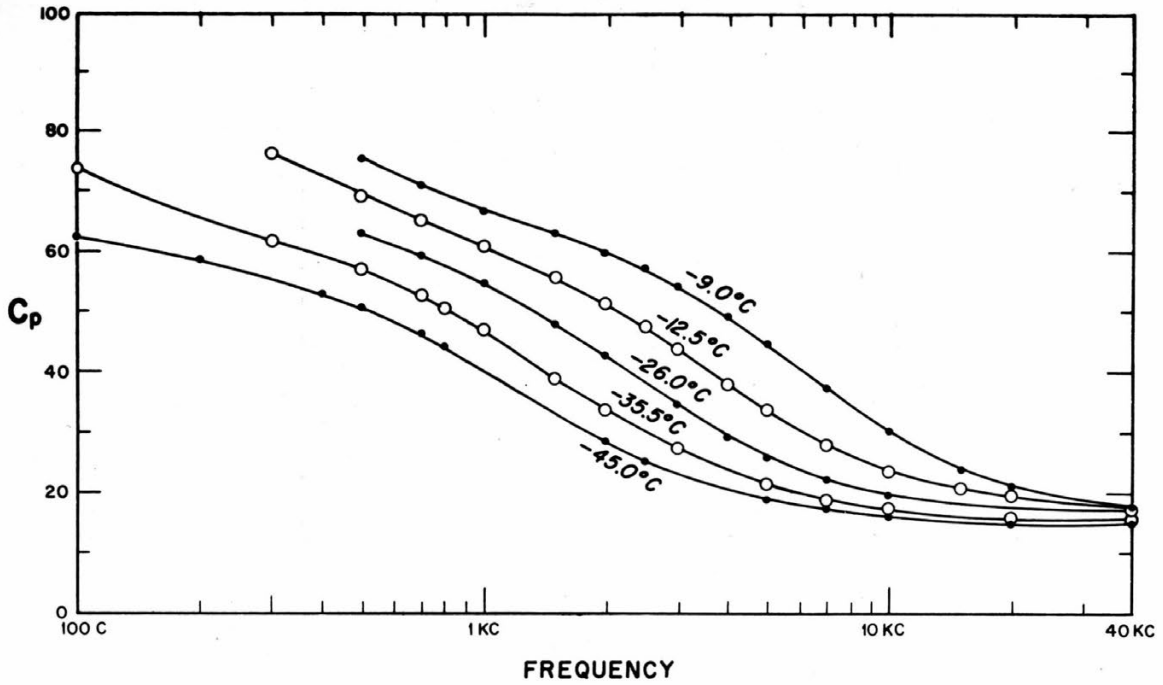

Figure 22a. Plot of the parallel capacitance C_p of the sample as a function of frequency for a single crystal containing 0.0025% NH_4F by weight. Various temperatures are indicated.

The data for the three different concentrations of Figure 21 are too scattered to allow meaningful individual analysis to be made on the basis of differences in concentration. However, one may fit the total data fairly well with an equation of the form

$$1/\tau = 3.3 \times 10^{15}\ e^{-13.5/kT} + 1.9 \times 10^{4}\ e^{-0.6/kT}.$$

The activation energies are 13.5 ± 1 kcal/mole and 0.6 ± 0.4 kcal/mole. The numerical factor will, of course, depend on the activation energy used. The first value for e, 13.5 kcal/mole, is close to that for pure ice as expected. However, it is noteworthy that the second is very different from the values of about 3.5 kcal/mole reported for more heavily doped polycrystalline samples by Brill et al. (1957). It would seem that two quite different processes are involved. It is not surprising that the data for the 0.00035% concentration sample exhibits behavior similar to that of pure ice over the range of temperature used. On the basis of the previous argument, we would expect to have to go to temperatures below -45C to see the transition region.

Figure 22b is of particular interest not because it shows different general values for different concentrations, since this may have been due to non-uniformity of sample dimensions, but rather because it indicates a decreasing value of $\epsilon_0' - \epsilon_\infty'$ with 1/T instead of an increasing value as is predicted by simple theory and as was found in the case of more heavily doped samples. Only for the highest concentration do we find a tendency to break away from this behavior, and the apparent change may well be due to the chance location of one or two points. Except for this feature, all three curves have nearly the same slope of 20K/1000. A possible interpretation is that many water molecules are somewhat frozen in position by the impurity molecules and are not susceptible to the slight externally applied polarizing field. Such behavior might occur if the NH_4F entered the lattice as NH_4^+ and F^- or NH_2^- and H_2F^+. Then the large electrostatic fields

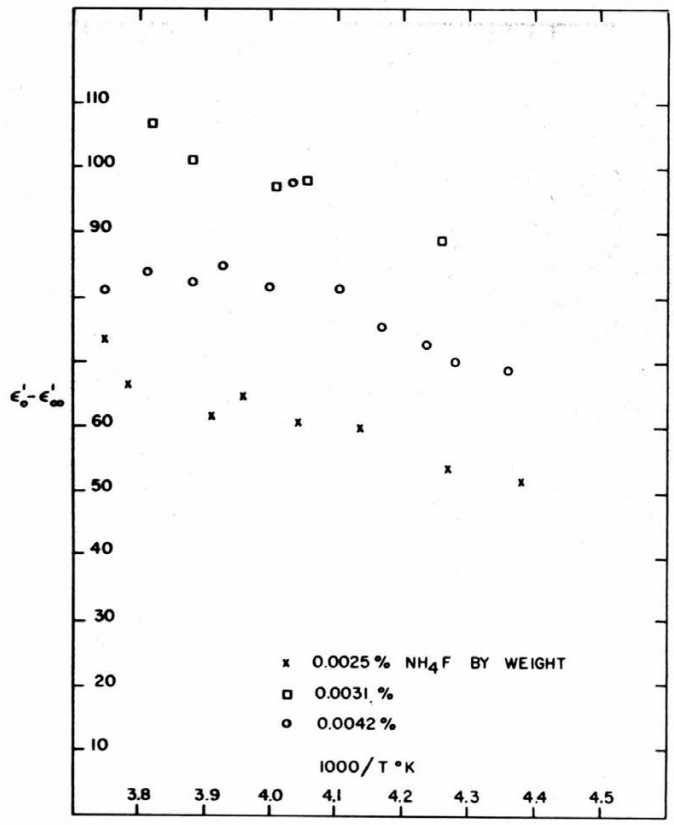

Figure 22b. Plot of $\epsilon_0' - \epsilon_\infty'$ as a function of 1000/T °K for the samples of Figure 21.

in the vicinity of the ions might hinder dipole rotation, this hindrance being more pronounced at low temperatures. Thus $\epsilon_0' - \epsilon_\infty'$ might be a function of the amplitude of the applied voltage. A very crude measurement of this kind was made on the 0.0031% sample which indicated an increase in $\epsilon_0' - \epsilon_\infty'$ of about $\frac{1}{2}$% for an increase in applied field from 1.5 to 34.5 v/cm.

The data of Figure 22b, replotted on a semi-log scale, yield values for the activation energy for the rate limiting process. The data for both the 0.0025% and 0.0033% samples suggest a process with an activation energy of 0.7 ± 0.1 kcal/mole. The data for 0.0042% are erratic but show a similar general trend. Within experimental error, this is the same activation energy as was found for the low temperature part of the dielectric relaxation time.

For the sake of completeness, the value of $\underline{R}_{dc}$ was measured for the 0.0042% samples as a function of temperature. The measurement was made by applying a voltage of 1.5 v to the sample and using a Keithley micromicroammeter to measure the current through the sample after it had dropped to a fairly steady rate. The data are plotted in Figure 23 and yield an activation energy of 18.1 kcal/mole. It should be pointed out that this method does not take into account polarization of the sample and so yields resistance values which are somewhat high.

Dielectric relaxation in pure ice; length effect

A series of experiments was conducted to determine the dielectric relaxation properties of one sample of single-crystal pure ice. This was done despite the rather extensive measurements on pure ice made by Cole and again by Scherrer and again

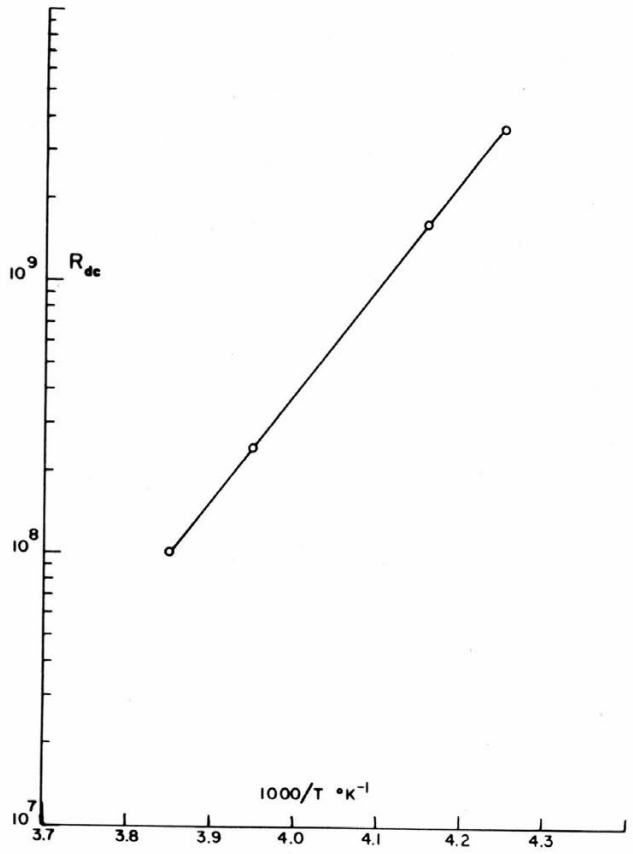

Figure 23. Semi-log plot of R_{dc} as a function of 1000/T °K for a single crystal of ice containing 0.0042% by weight of NH_4F.

several years ago by Feuersanger, because the method of sample preparation was unique.

The sample was grown in a tube containing four transverse platinum grids. The c-axis of the crystal was along the tube axis and the crystal was grown through the grids, maintaining its single crystal structure despite them. The grids were so placed that the distance between the first two was 0.5 cm, that between the second and third 1 cm, and that between the third and fourth was 1.5 cm. Thus we were able to measure the properties of three samples of the same single crystal, each of which was of a different length and none of which had been machined or handled in any way. In addition, it was felt that the use of grid electrodes buried in the ice would help reduce such polarization problems as might be present. Moreover, during the growth of this crystal, the growth currents had been monitored by connecting to a micromicroammeter pairs of grids which bracketed the liquid-solid interface. Thus they had been effectively shorted and the crystal had been grown in a field free region.

Figure 24 is a semi-log plot of the relaxation time τ versus 1000/T°K. The solid line is an average of literature values and the points are our data (c-axis perpendicular to the grids). The temperature was measured by means of a thermistor bridge (described in the Appendix) which was specially calibrated for this experiment against a standard platinum resistance thermometer. The calibration of the thermistor thermometer is believed accurate to ±0.05C but since it was necessary to mount the sensing

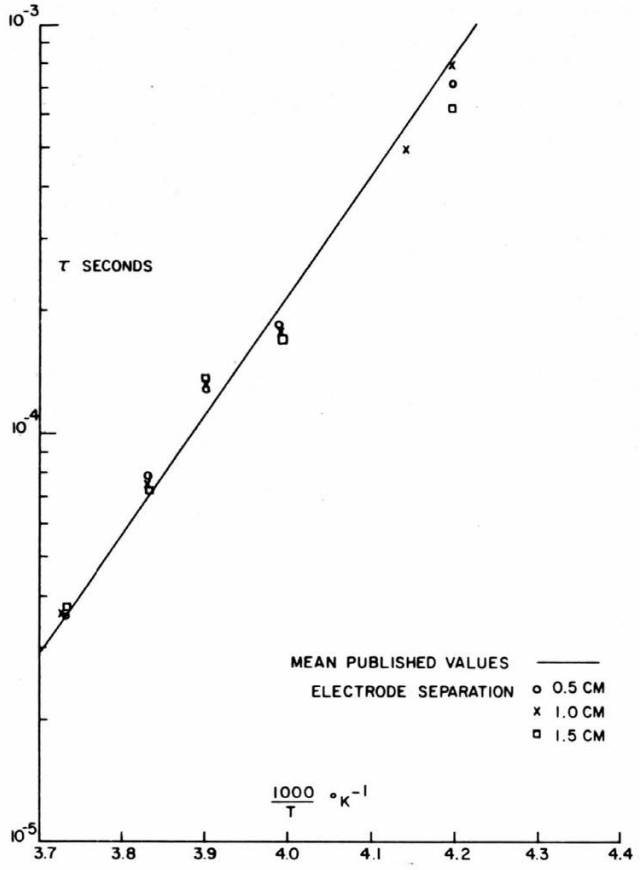

Figure 24. Semi-log plot of the relaxation time of pure ice as a function of 1000/T °K for samples of three different lengths from the same single crystal.

element on the outside wall of the Lucite tube containing the sample, the temperature is in doubt by ±1C.

It can be seen that the agreement with the published data is good and therefore there is no striking difference between this and other samples. It is also evident from the excellent grouping of the points for different sample lengths that sample length is not a factor. Good Cole plots were obtained throughout and the centers of the circles were consistently below the c' axis by about 10% of the value of c'' at f_{max}.

Long-period dielectric effects

When an ice dielectric condenser which has been charged for a long time is discharged, the discharge current does not follow a simple exponential law (Brill and Camp, 1961, p. 70-74). Instead, there is an immediate discharge of a more or less exponential character followed by a small current which persists for many hours. This current decays gradually and the form of the decay curve is complicated.

A brief report of some early experiments of this kind was given in CRREL Report 68. It was pointed out there that the decay curves measured for times as long as several hours could not be analyzed as the sum of exponential terms without using at least four such terms. Similar behavior was observed for both single crystal and polycrystalline material and the general observations were the same whether the charging potential was applied to the measuring condenser after the sample had been grown or while the ice was freezing in the condenser. Of particular interest was the

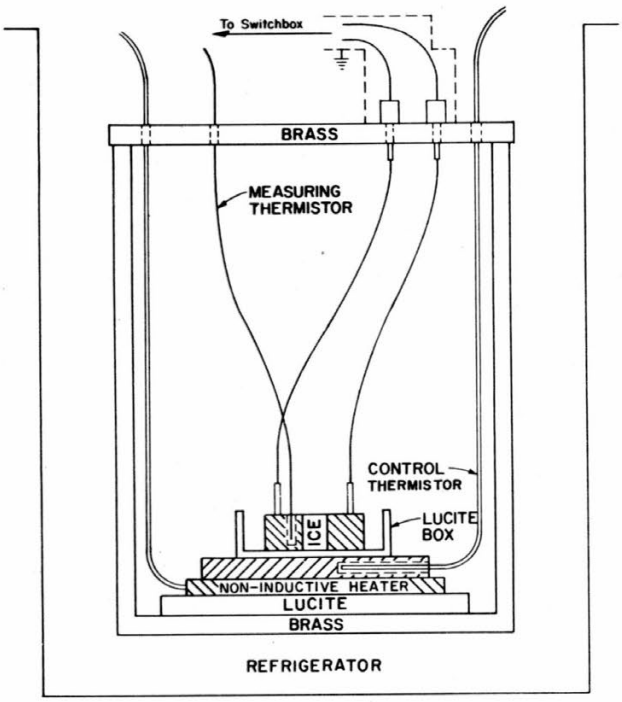

Figure 25. Thermostatically controlled sample holder for dielectric tail experiments.

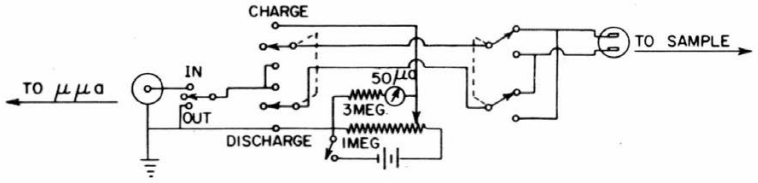

Figure 26. Circuit diagram of switch and charging box for long-period dielectric effect studies.

fact that if a condenser were first charged for a long time in one polarity, then discharged briefly and recharged in the opposite direction for a short time, and finally discharged again, the final discharge current decayed to zero, reversed polarity, and approached asymptotically the long-time decay curve characteristic of the first charging.

Many difficulties were encountered in this early work and it has been necessary to revise the apparatus substantially. One major problem was maintaining constant temperature for many hours. The revised apparatus is shown in Figure 25.

The sample is mounted between gold-plated brass electrodes, one of which contains a thermistor for temperature measurement. Temperature is controlled by a heater directly beneath the sample. The heater is controlled by a second thermistor driving a Fenwal series 560 control unit. Temperature stability of ±0.25C was obtained for short periods of time and ±1C for periods of many hours. The data are recorded by means of a Keithley micromicroammeter driving a Varian strip chart recorder.

Another improvement was the construction of a well-shielded switch box (Fig. 26) which contained the charging batteries and featured very low leakage switches. The leakage current with the switches set for charge at the full 120 v potential was

5×10^{-11} amp, a negligible value. Charge and discharge curves were measured with the sample holder clean and empty in order to determine the capacitance and leakage of the sample holder and connecting cables. The time constant for these curves was found to be 1.1 sec which is about the balancing time of the recorder. The major source of error was the Keithley model 410 micromicroammeter which introduced an absolute uncertainty of the order of ±5%. Relative measurements were very much better, perhaps 1% overall.

The temperature was monitored by means of a thermistor bridge of our design using a Veco 31A2 thermistor as a sensing element. This unit has proved so useful that it is described in the Appendix. At the time of these measurements, the thermistor had been calibrated against a precision thermometer only to an accuracy of ±0.5K but a change of temperature of 0.01K could be measured.

Polycrystalline ice samples were prepared by freezing commercial distilled water in the condenser, which consisted of two gold-plated brass blocks mounted in a Lucite box so that their opposing faces were parallel and separated by 0.65 cm. The area of the faces was 2.3 cm^2. Gold plating was found to be necessary in order to avoid corrosion of the blocks. The single crystal experiments were performed on samples cut from Alaskan glacier ice and mounted in the same capacitor. The plates were frozen to the crystal.

Measurements of charge and discharge currents were made on five different polycrystalline samples and five different experiments were performed on one sample of single-crystal glacier ice. The latter was mounted so that the electric field was perpendicular to the c-axis of the crystal. The results are perplexing in that, although the actual numbers are not very reproducible, both charge and discharge curves for both single crystals and polycrystals can be fitted fairly well by an expression of the form

$$i = at^{-\alpha} e^{-bt} \qquad t > 1 \text{ sec} \tag{20}$$

where i is current, t is time and a, b, and α are constants having different values for each sample. The term $t^{-\alpha}$ is dominant over several orders of magnitude and the plot of log i vs log t therefore is linear in this interval (e.g., 1 to 1000 sec). The range of values for the constants is given in Table II. The overlap in results is so large that no pattern emerges for single crystal ice as distinct from polycrystalline ice.

Table II. Values of the constants in eq 20.

	a (amp)	b (sec^{-1})	α
Charge curve	10^{-6} to 10^{-8}	6×10^3 and larger	0.030 to 0.15
Discharge curve	3×10^{-8} to 10^{-9}	10^4 and larger	0.014 to 0.47

Typical charge and discharge curves are given for polycrystalline samples in Figures 27 and 28 and for a single crystal sample in Figures 29 and 30. The latter are particularly interesting in that they show the effect of successive charging of the sample for progressively longer times (10 sec, 30 sec, 60 sec, and 300 sec). All of these measurements were made at -16.0 ± 0.3C. It is gratifying that the charging curves are all very nearly the same. The initial charging current for the original sample may be a few percent higher than the others as might be expected. But the agreement is within the bounds of known experimental error. The discharge curves are also quite similar, with differences becoming more pronounced as time goes on. Thus the current is better sustained if the sample has been charged for a longer time.

A number of pieces now begin to fall into place. The very complicated expressions needed to describe the decay process suggest that more than one mechanism is involved. Even more persuasive of this hypothesis is the "memory" noted earlier by which a condenser charged originally with one polarity and then recharged briefly with the opposite

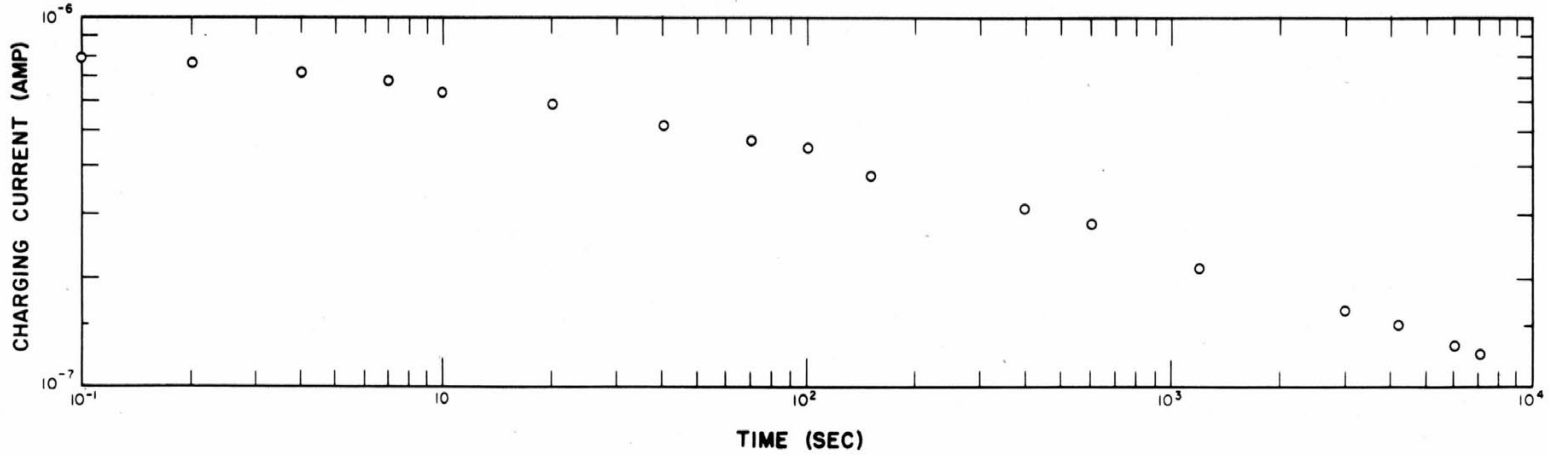

Figure 27. Typical charging current curve for polycrystalline sample.

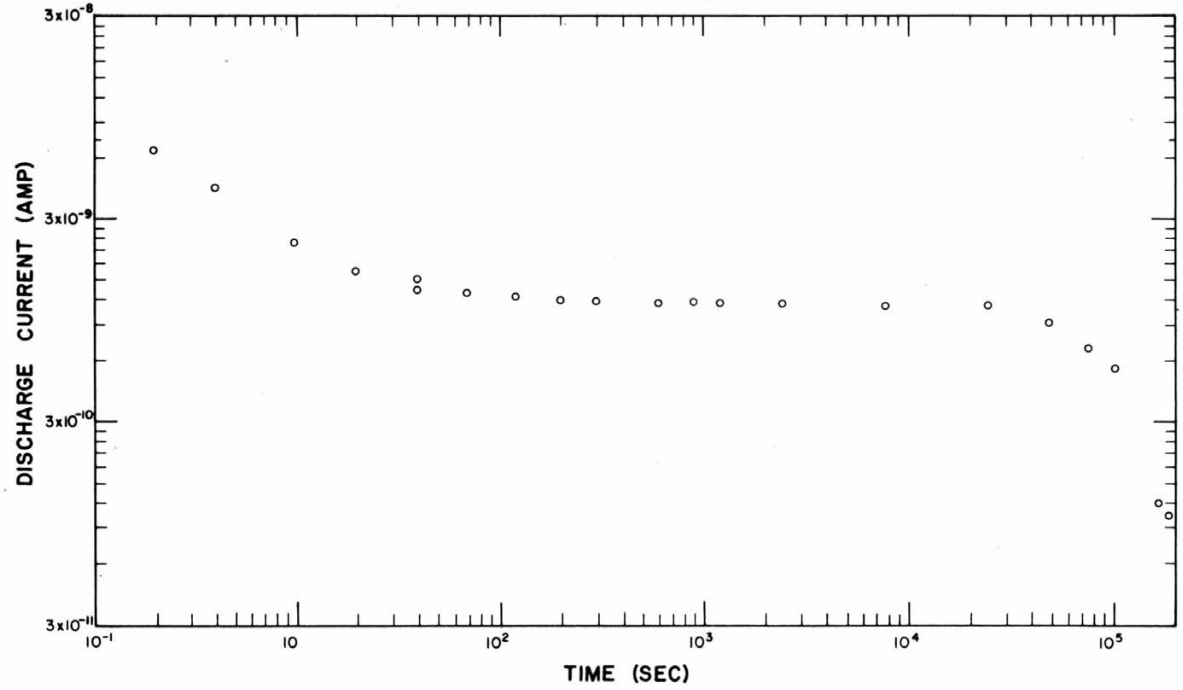

Figure 28. Typical discharge curve for polycrystalline sample.

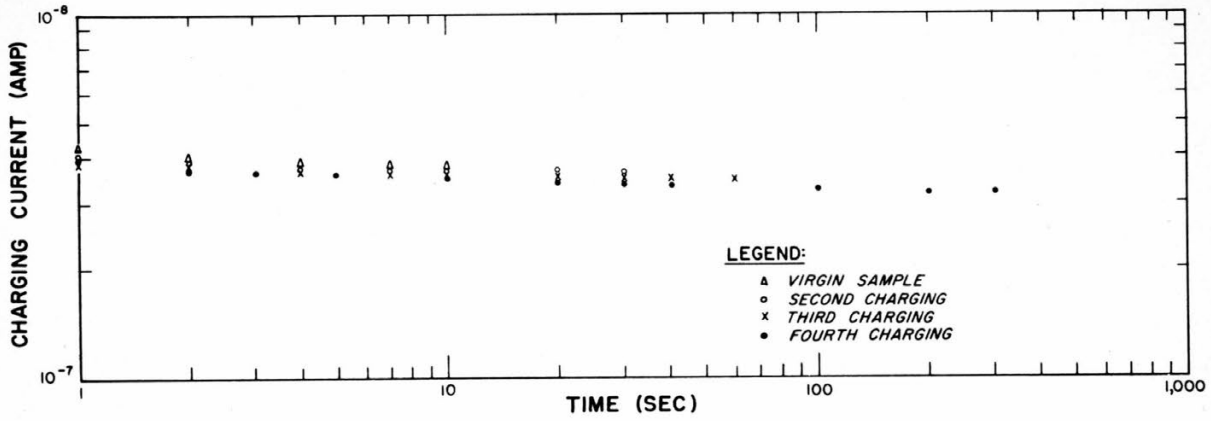

Figure 29. Charging curves for single crystal. After each charging run, the crystal was discharged for an extended time (Fig. 30). Successive charging periods were for longer duration.

polarity shows a reversal of its discharge current. There must therefore be one process which dominates the first 3 to 30 sec and another which determines the long-time behavior. The activation energy of the long-time process can be measured at least roughly because the current is changing so slowly with time. It is possible to vary the temperature and measure the effect on discharge current. This has been done but our inability to change sample temperature abruptly makes the results rather uncertain. We estimate the activation energy as 21 ± 5 kcal/mole. A similar estimate made by changing the temperature during the initial part of the discharge leads to an estimate of 6 ± 3 kcal/mole, again indicating a very different process. Decroly, Granicher, and Jaccard (1957, p. 465) have shown that the passage of a direct current through ice will cause hydrogen to be liberated at the cathode. Thus one is tempted to ascribe the second process to electrolysis and the formation of an electrolytic cell in the charging process. The 21 kcal/mole may then be the activation energy for the diffusion of hydrogen through the ice. The first process remains a mystery. Clearly a better determination of the activation energies of these processes is an important matter to pursue.

The electrolysis hypothesis is perhaps weakened by the observation that in no case did the total charge which flowed in the external circuit upon discharge clearly exceed that which would be caused by the transfer of one electron per surface oxygen atom from one condenser plate to the other. In some cases, the charge which flowed during the charging process was greater by about a factor of ten than this amount. Of course, an electrolytic process which is reversible only in regard to a monolayer of ions is a possibility.

OPTICAL EXCITATION OF BJERRUM DEFECTS

An essential feature of the theory of the dielectric properties of ice is the existence of Bjerrum defects (Granicher, et al., 1957). In fact, the relaxation time for pure ice is inversely proportional to the number of these defects. Stated in terms of our equivalent circuit (Fig. 18), C_S depends on the total number of molecules and not on the number of defects while R_S depends on the number of defects as well. (The conductivity is proportional to the concentration of Bjerrum defects.) Therefore, it would seem possible to investigate, by electrical measurement, properties such as the lifetime of these defects if they could be produced in the sample in non-equilibrium numbers. A series of experiments has been performed in which an attempt has been made to produce Bjerrum defects optically. The results have been interesting and unexpected.

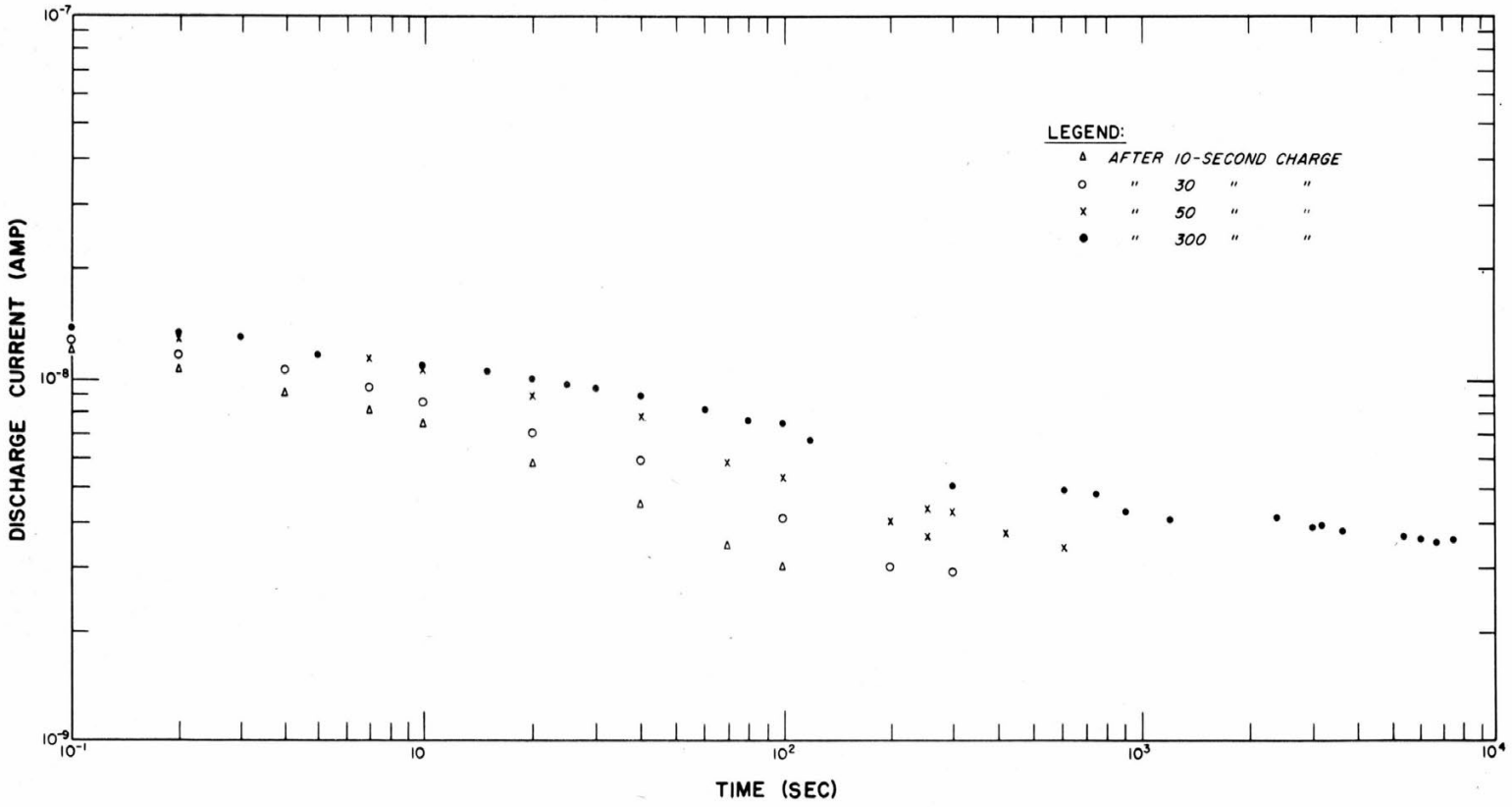

Figure 30. Discharge curves for single crystal sample after charging shown in Figure 29.

In order to produce significant effects, one might expect to have to produce a density of defects comparable to equilibrium density. Granicher has calculated this number and finds the density at -10C to be between 2×10^{15} and 4×10^{13} /cm^3. The activation energy to produce these defects is about 25 kcal/mole (1.1 ev). Thus irradiation with light of wavelength shorter than 2.38 μ should produce them, and a peak in efficiency would be expected at about this wavelength. Ockman (1958, p. 204) has reported an absorption peak for ice from about 7.5 to 8.2 $\times 10^3$ wave numbers which covers this range. The absorption coefficient reported is 1.6 to 2.2 cm^{-1}. Thus most of the effect will be in the first few millimeters adjacent to the crystal surface.

Rough calculations indicate that a black body at 2300K will give about 10^{15} photons/sec incident on the sample per watt of source power. This figure allows a factor of 10 for geometry. The effectiveness of photons in producing a detectable change will depend, of course, upon the efficiency of defect production and on the lifetime of the defects.

Our first experiments were carried out using a condenser made of a circular metal plate of 2.5 cm diam, inside a slightly larger ring. The spacing between, about 0.5 mm, was filled with polycrystalline ice to a depth of about 1 mm. This sample was connected to an a-c reactance bridge (GR 716C) and the bridge was balanced at 1 kc. Illumination by a strong (30-w) microscope illuminator produced no observable effect.

In order to experiment with much more intense light, it has been necessary to use a flash technique. This has two distinct advantages. First, much more intense sources are available for pulse illumination than for steady illumination and, second, the duty cycle can be made small enough so that sample heating is slight. In the pulse experiments we balance the bridge and then detect the transient unbalance by means of an oscilloscope whose sweep was triggered a moment before the light was flashed.

In our first experiments using pulsed light, we used fine wires exploded by a large current pulse to generate the flash. The apparatus is shown in Figure 31. Two long rectangular ice capacitors were connected in parallel and mounted one on each side of a hairpin-shaped wire. The capacitor plates are on the top and bottom so the light penetrates the ice. The ice bars were approximately 5 mm by 5 mm by 70 mm long. A hairpin-shaped wire light source was used to minimize inductance and to reduce the electrical coupling between the light circuit and the measuring circuit. Using this apparatus, transient unbalance signals such as Figure 32 were obtained. However, the exploding wires were not very reliable as light sources and so Sylvania M-2 flashbulbs were used instead. The use of flash bulbs required further modification of the ice capacitor; Figure 33 shows the interlocking comb arrangement which was finally used. Ice fills the space between the combs. This region is about 1 mm wide by 1.8 mm deep by 56 cm in total length. Polycrystalline samples are made by placing the capacitor in a Lucite box, just covering the plates with water, and allowing it to freeze. Single crystal samples are mounted by allowing the tines to melt partially into a slab of the crystal to be studied and then refreezing. The flash bulb is mounted in a reflector directly above the capacitor. The end of the bulb is about 5 mm from the surface of the condenser. This arrangement has been found to give reproducible results and a number of measurements have been made using the bridge technique described above. Recently we have conducted also a set of d-c experiments in which the sample, a 45 v battery and a d-c oscilloscope (2 meg input resistance) are all connected in series. The oscilloscope is balanced to compensate for the sample dark resistance and then the sweep and flash are synchronously triggered. The resulting transient is photographed as in the a-c method.

Before discussing the results of these experiments it is well to say a few words about the relative merits of a-c and d-c techniques. As we now know from the dielectric relaxation and the dielectric "tail" experiments, the complete electrical analogue of an ice capacitor is very complicated. There will be a series $\underline{R}_s$, $\underline{C}_s$ for the audiofrequency relaxation, a parallel $\underline{C}_\infty$ for the high-frequency dielectric constant, a parallel d-c conductivity σ and probably another low-frequency (1/10 cycle or so) relaxation represented by a series RC circuit in parallel with the first as shown dotted in Figure 34. From a

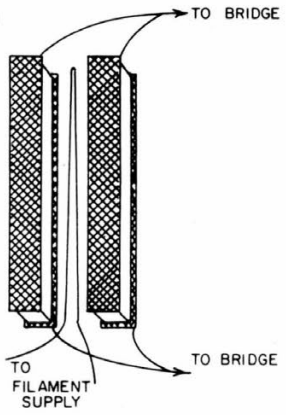

Figure 31. Exploding-wire light-pulse apparatus.

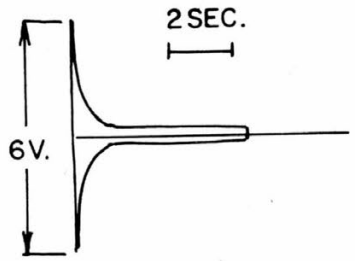

Figure 32. Transient unbalance produced by exploding-wire technique.

Figure 33. Capacitor for optical experiments using flash bulbs as a light source.

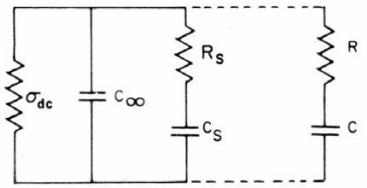

Figure 34. Possible "complete" electrical analogue of ice-filled capacitor.

d-c experiment, only those phenomena associated with σ_{dc} are expected. However, a pulsed d-c experiment would give a transient resulting from changes in any or all parameters of the circuit. While it may be possible to separate the contributions somewhat in terms of characteristic times, the separation is complicated by the transient associated with the lifetime of the defects themselves. An a-c experiment at audiofrequencies should be much simpler to interpret, for unless they are very large, transient changes in σ_{dc}, R, and C should not alter the audiofrequency impedance of the circuit. Since C_∞ and C_S are independent of the concentration of Bjerrum defects, all the signal should result from the changes in R_S. The argument against a-c measurements is the fact that the unbalance of the bridge reflects both phase and amplitude change. The results are thus difficult to interpret. However, for a small change (ΔR) in R, the amplitude of the deflection should be proportional to ΔR. This was checked experimentally using an equivalent circuit and was found to be the case.

The real difficulty comes about because the constant of proportionality is a function of frequency and of R_S. Since the latter varies with temperature, it is difficult to compare measurements at different temperatures. Calculations indicate that, if the bridge unbalance is due to a change in R_S, the constant of proportionality should be largest at some intermediate frequency and fall off toward zero at low and high frequency. Actually, shunt capacitance also will cause it to fall off at high frequency. Similarly, since $\omega_m = \frac{1}{R_S C_S}$ increases with increasing temperature, the constant should be small at high temperature (at a fixed frequency) and rise as the temperature is lowered.

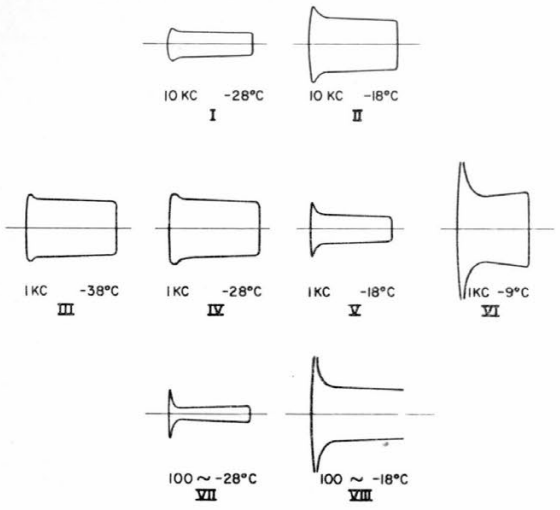

Figure 35. Effect of temperature and frequency on transient bridge unbalance caused by light pulse. Note: the gain is the same for all figures except 1 kc -38C and 1 kc -28C.

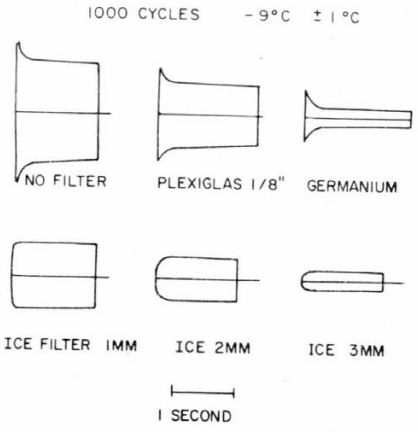

Figure 36. The effect of various filters on the transient bridge unbalance in the a-c optical experiments. Gain settings are the same for all pictures except the germanium filter which is 4 times larger.

Figure 35 shows a tracing of a typical set of photographs of the unbalance signal versus time for one sample at constant temperature for various frequencies and for different temperatures with constant frequency. The oscilloscope gain was the same in all of these experiments with the exception of III and IV (for which it is uncertain) and the total sweep time for each was about 1.5 sec. For discussion purposes, the initial sharp peak is referred to as the pulse and the final plateau as the step.

Inspection of Figure 35 shows that the temperature-frequency behavior of the pulse is quite the reverse of what we have predicted above. The pulse is largest for high temperature and low frequency. Its time constant ($\sim$ 50 ms) seems to be independent of both, although the limits of error in determining this are large. The step also seems to be quite independent of frequency. Such variation as does occur exhibits no discernible pattern and has been ascribed tentatively to variations in light output due to irregularities in the bulbs and frosting of the surfaces. However, there does seem to be an increase in step height with increasing temperature.

These experiments suggest that the pulse results not just from a change in $\underline{R}_S$ but rather from a change in a conductance in parallel with the series $\underline{R}_S\underline{C}_S$ combination. The apparent frequency independence of the step is perplexing in that the sample impedance as a whole does vary with frequency. It may be that it represents two compensating phenomena such as a simultaneous change in $\underline{R}_S$ and in a parallel conductance. However, the experimental data are too sparse to warrant much speculation.

In order to try to isolate the spectral region producing these effects, a series of experiments was run in which the frequency and temperature were held constant and different filters were interposed between the sample and the light source. Figure 36 shows some of the results. A glass filter which cut off wavelengths greater than 5 μ had no effect. A Plexiglas filter $\frac{1}{8}$ in. thick, which should have cut out nearly all radiation with wavelengths longer than 2.1 μ and attenuated increasingly from 1.5 to 2.1 μ, cut down the pulse by the factor 1.8 and the step by 1.5. Calcuations indicate that only 30% of the radiation from a black body at 3800K would be eliminated by such a filter. Since the average temperature was probably somewhat lower, we would expect this to represent a minimum percentage.

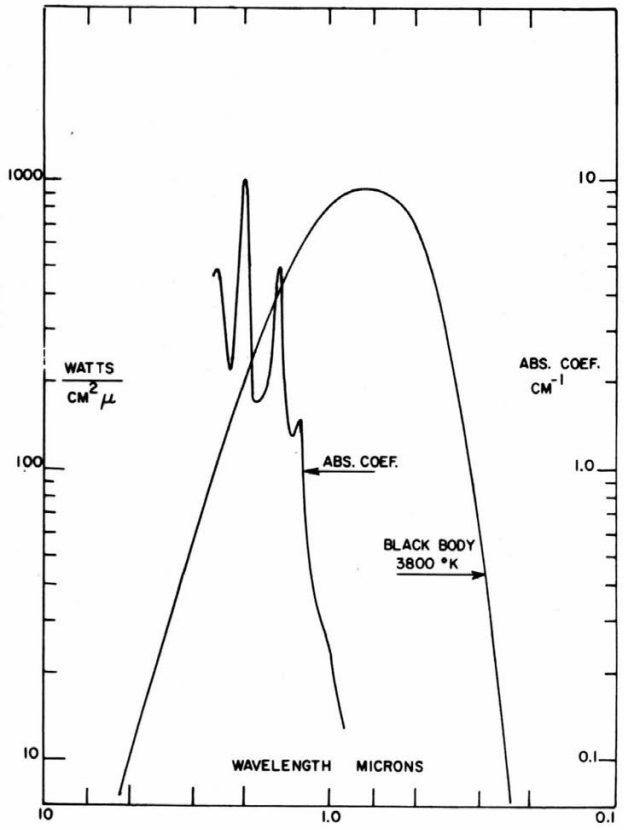

Figure 37. Absorption coefficient for ice superimposed on the spectral distribution curve for a black body at 3800K.

A germanium filter, which should have removed all radiation of shorter wavelength than 1.8 μ and reduced all the transmitted radiation 50% because of reflections at the surfaces, reduced the pulse by a factor of 3 and the step by a factor of 4.3. Taken together, the results of these two experiments suggest that the pulse is produced by wavelengths somewhat longer than those producing the step and that both regions are in the vicinity of 1.8 μ. (Note that the germanium filter would be expected to cut out about 88% of the total energy.)

A silicon filter which cut off all radiation $\lambda < 1$ μ attenuated both pulse and step equally. But the surface of this filter had been ground and, therefore, it probably resulted in very large attenuation overall, masking any differences which might have accrued.

A 1-mm sheet of ice between the source and the sample is enough to completely destroy the pulse without very serious attenuation of the step. Greater thicknesses appreciably reduce the step. But note in addition the rounding of the leading edge. The rise time of the step under these conditions is comparable to the decay time of the pulse in the case of no filter.

Finally we must look again at the absorption coefficient of ice in the region of interest. Figure 37 shows Ockman's values of the absorption coefficient for pure ice superimposed on the spectral distribution curve for a black body at 3800K. There are two important peaks in the region being considered, one at about 1.5 μ and one at about 2 μ. It is quite in keeping with the experimental evidence that there are two processes

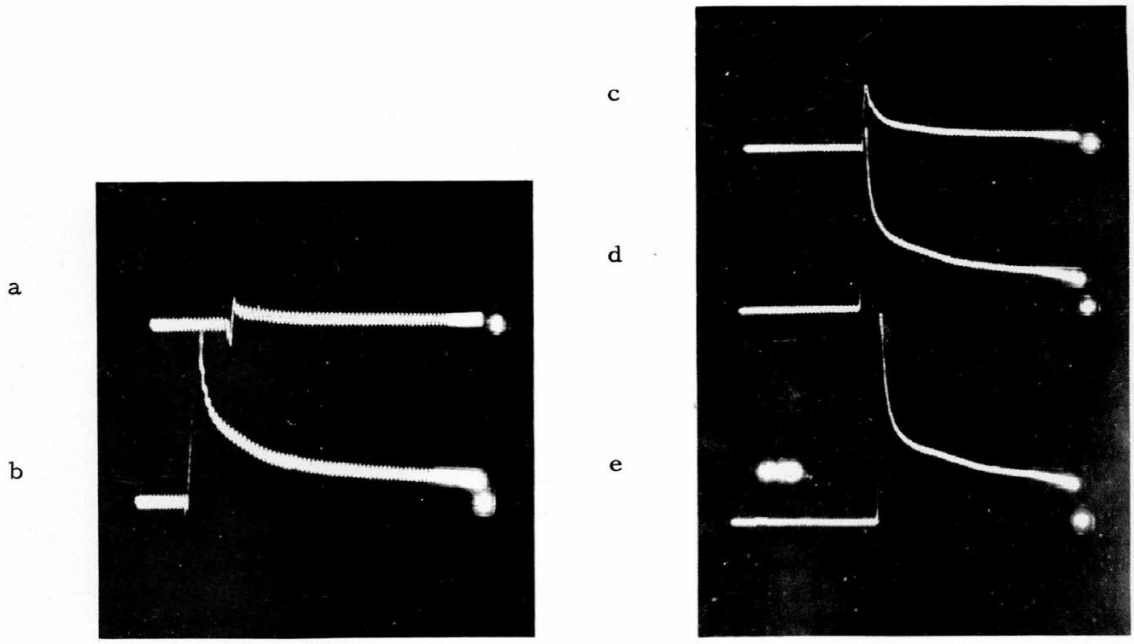

Figure 38. Photograph of oscilloscope traces in several d-c experiments performed at different temperatures. The higher temperature runs have been attenuated as follows:

(a) -37.6C, Att. x 1;
(b) -30.8C, Att. x 1;
(c) -20.0C, Att. x 10;
(d) -22.5C, Att. x 10;
(e) -18.5C, Att. x 20.

to be considered. One gives rise to the peaks and is due to the 2 μ absorption, while the other gives rise to the step and is due to the peak at 1.5 μ. It is also clear that the 2 μ process is more nearly a surface phenomenon than is the 1.5 μ process.

A tempting hypothesis is that the pulse represents flash heating of a surface layer which then transfers its heat to the bulk in about 50 ms. Calculations indicate that heating of a surface layer 1/10 mm thick by a few degrees centigrade could alter the conductivity of a 1 mm sample so as to give rise to a pulse of the height observed. Furthermore, the time constant for the decay of temperature in this surface layer would be about 50 ms. However, calculations also indicate that, to the first approximation, the total conductance is independent of whether the heat is concentrated in a surface layer or spread throughout the sample. Therefore, we cannot account for the pulse in this way.

On the other hand, it appears that we must relate the step to bulk heating because the time constant for the decay of the step is several minutes, which is long enough for cooling to take place and, more convincing, it depends on whether or not the air in the refrigerator is circulating. When the fan is on, the time constant is shorter.

Because of the success of the low frequency experiments, a set of d-c experiments was also performed. The sample was mounted as in the a-c experiments but it was connected in series with a 45 v battery and a d-c oscilloscope (input resistance 2 meg). The oscilloscope deflection was balanced and the light was flashed. The deflection which then resulted was that caused by the light. Figure 38 shows a series of such measurements made at different temperatures. The deflection is very similar to that observed with a-c, having a pulse of about the same time constant and a step. Although the

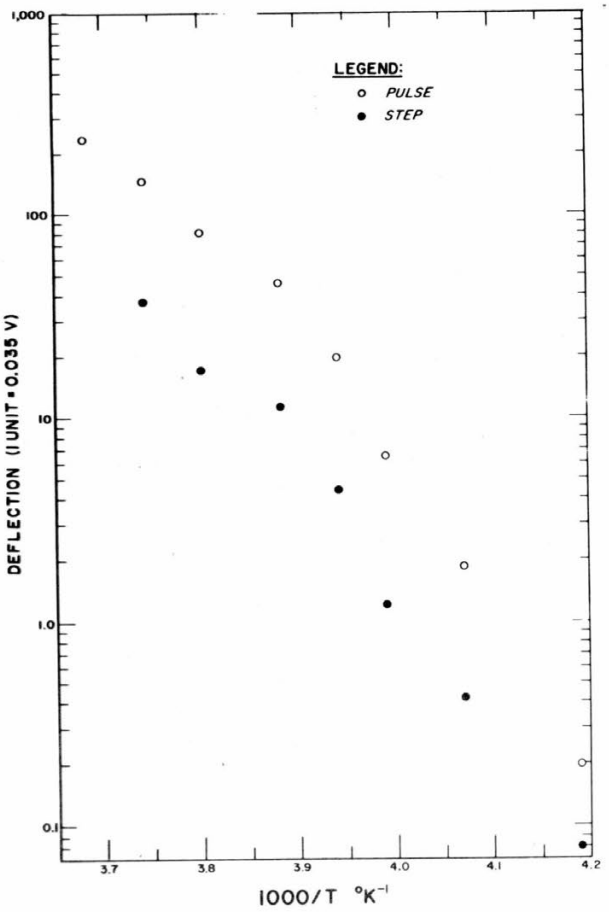

Figure 39. Semi-log plot of pulse height and step height as a function of 1000/T.

experimental fluctuation due to variation in bulbs and perhaps frosting of bulb and sample may be large, these data have been used to obtain Figure 39, a semi-log plot of step height and pulse height versus 1000/T. The activation energy which results, 38 kcal/mole, must be regarded with some suspicion for the reasons just mentioned. At any rate, an activation energy much higher than those associated with a conduction or dielectric relaxation in pure ice seems to be involved. To consider the implication of this result, we must perform a few calculations.

In the d-c case, the conductance of the sample, σ, is in series with the input resistance of the oscilloscope, r. The voltage, V, across r is balanced out and the change in this voltage due to a change $\Delta\sigma$ in σ is measured. If E is the total applied voltage, then

$$V = \frac{E\, r\, \sigma}{r\sigma + 1} \qquad \text{and} \qquad \Delta V = \frac{E\, r\, \Delta\sigma}{(r\sigma + 1)^2} .$$

Assume $\sigma = A\, e^{-\epsilon/kT}$, where A is constant and ϵ is activation energy for the conduction process.

Case 1 Bjerrum defects optically injected.

$\Delta\sigma$ = constant independent of temperature.

Then for $r\sigma << 1$

$\Delta V = Er\Delta\sigma$, independent of temperature.

For $r\sigma >> 1$

$$\Delta V = \frac{E\Delta\sigma}{r\sigma^2} = \frac{E}{rA^2} \; e^{2\epsilon/kT} \Delta\sigma.$$

But this requires that ΔV decrease as temperature increases, contrary to experiment.

Case 2 Adiabatic heating of the sample (ΔT = constant) or of the surface.

$$\Delta\sigma = \left(\epsilon/kT^2\right)\sigma \; \Delta T.$$

In the case of surface heating of a layer of thickness d on a sample of thickness D, this will be

$$\Delta\sigma = \frac{d}{D} \; \frac{\epsilon}{kT^2} \; \sigma \; \Delta T.$$

$$\text{For } r\sigma << 1, \; \Delta V = \left(Er \frac{d}{D} \; \frac{A\epsilon}{k} \; \Delta T\right)\left(e^{-\epsilon/kT}\right)/T^2$$

and ΔV increases with temperature with an activation energy ϵ so long as $\epsilon > 2kT$.

$$\text{For } r\sigma >> 1, \Delta V = \frac{E \epsilon d \Delta T}{r k D A} \; \frac{e^{\epsilon/kT}}{T^2}$$

and again ΔV decreases as temperature increases.

Thus using the simple series model, the case of surface (or bulk) heating is the only one which leads to an acceptable temperature behavior and this requires an activation energy for σ which is very much greater than that reported by Scherrer. Moreover as we have already said, the conductance should be the same whether we raise the whole sample $\theta°$ or a fraction d/D of the sample (D/d) $\theta°$ and so we cannot account for the pulse.

The simple series a-c case has already been disposed of as giving the wrong frequency behavior. But if defects are injected, we can expect both σ_{dc} and $R_s = 1/\sigma$ to be changed. Thus we must consider the circuit of Figure 40. To simplify the analysis,

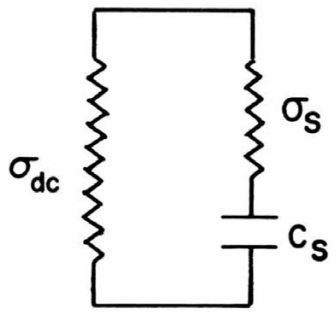

Figure 40. Simple circuit used as analog for the a-c pulsed light experiments.

we will consider only the extreme high frequency and low frequency cases. Since the unbalance current in the bridge will be proportional to the $\Delta y/y$ where y is the complex admittance of the whole circuit, we have for high frequency

$$y \rightarrow \sigma_{dc} + \sigma_s$$

and for low frequency

$y \rightarrow \sigma_{dc}$.

Assume $\Delta\sigma_{dc} = \Delta\sigma_s$ and $\sigma_s = A_1 e^{-\epsilon_1/kt}$ $\sigma_{dc} = A_2 e^{-\epsilon_2/kT}$

Case 1 Injected defects $\Delta\sigma_{dc}$ = constant.

High frequency $\frac{\Delta y}{y} = \left(\Delta\sigma_{dc} + \Delta\sigma_s\right)\Big/\left(\sigma_{dc} + \sigma_s\right)$.

Low frequency $\frac{\Delta y}{y} = \Delta\sigma_{dc}/\sigma_{dc}$.

Thus if $\sigma_{dc} = \sigma_s$ and $\Delta\sigma_{dc} = \Delta\sigma_s$, the unbalance will be the same at high and low frequencies. However, we have neglected here the parallel capacitance of the leads etc. which will attenuate the signal severely at high frequencies. In any event, the temperature dependence will be the inverse of that of σ_{dc} and σ_s, which is contrary to experiment.

Case 2 Adiabatic heating $\Delta\sigma_s = \frac{\epsilon_1}{kT^2}\ \sigma_s\ \Delta T$ and $\Delta\sigma_{dc} = \frac{\epsilon_2}{kT^2}\ \sigma_{dc}\ \Delta T$.

At high frequency, $\frac{\Delta y}{y} = \frac{\Delta T}{kT^2}\ \frac{\sigma_{dc}\epsilon_2 + \sigma_s\epsilon_1}{\sigma_{dc} + \sigma_s}$. At low frequency, $\frac{\Delta y}{y} = \frac{\Delta T}{kT^2}\ \epsilon_2$.

Again, if $\epsilon_1 = \epsilon_2$, the high and low frequency behavior should be the same except for the shunting at high frequencies due to the parallel capacitance. But again, the temperature dependence is unsatisfactory.

In summary then we apparently have two processes to consider. One gives rise to the pulse and is associated with the absorption of longer wavelengths, possibly the 2 μ band. Since the absorption coefficient for this process is high, it must occur most strongly near the surface. The attenuation at high frequencies is understandable in terms of shunt capacitance, and the persistence of the effect at low frequencies suggests the inclusion of a parallel conductance which is also affected. The observed temperature dependence would seem to exclude injection of Bjerrum defects as a dominant factor at least for the simple model presented here. However, simple heating also seems to fail in accounting for the magnitude of the activation energy found for the d-c experiments. In the event that injection of Bjerrum defects is the dominant mechanism, their lifetime is of the order of 1/20th sec. The process which gives rise to the step is apparently associated with bulk heating and the absorption of shorter wavelength radiation, possibly 1.5 μ. However, here again the activation energy is much too large. It must remain for further more refined experiments to provide an answer.

REFERENCES

Borrmann, G. (1941) Physik, Z., vol. 43, p. 147.

Brill, Rudolf (1957) Structure of ice, U. S. Army Snow, Ice and Permafrost Research Establishment, Corps of Engineers, SIPRE Report 33, 67p.

_____ and Camp, Paul R. (1961) Properties of ice, USA SIPRE, Research Report 68, 75p.

Cole, K. S. and Cole, R. H. (1941) Dispersion and absorption in dielectrics. I. Alternating current characteristics, Journal of Chemical Physics, vol. 9, p. 341-351.

Decroly, J. C., Grãnicher, H., and Jaccard, C. (1957) Caractère de la conductivite electrique de la glace (Characteristics of the electrical conductivity of ice), Helvetica Physica Acta, vol. 30, p. 465-467.

REFERENCES (Cont'd.)

Gränicher, H., Jaccard, C., Scherrer, P., and Steinemann, A. (1957) Dielectric relaxation and the electrical conductivity of ice crystals, Discussions Faraday Society, no. 23, p. 50-62.

Jakob, M. and Erk, S. (1928) Wärmedehnung des Eises zwischen 0 and -253°C (Thermal expansion of ice between 0 and -253°C), Zeitschrift fur die Gesamte Kälte-Industrie, vol. 35, p. 125.

James, R. W. (1950) The optical principles of the diffraction of X-rays. London: G. Bell and Sons, Ltd.

Kittel, Charles (1956) Introduction to solid state physics, 2nd edition. New York: John Wiley and Sons, 617p.

Landauer, J. K. (1958) The growing of large single crystals of ice, USA SIPRE, Research Report 48, 7p.

Lang, A. R. (1958) Direct observation of individual dislocations by X-ray diffraction, Journal of Applied Physics, vol. 29, no. 3, p. 597-598.

La Placa, S. and Post, B. (1960) Thermal expansion of ice, Acta Crystallographica, vol. 13, no. 6, p. 503-505.

Lonsdale, K. (1958) The structure of ice, Proceedings of the Royal Society (London), series A, vol. 247, p. 424-434.

Ockman, N. (1958) The infra-red and Raman spectra of ice, Advances in Physics, vol. 7, no. 26, p. 199-220.

Powell, R. W. (1958) Preliminary measurements of the thermal conductivity and expansion of ice, Proceedings of the Royal Society (London), series A, vol. 247, no. 1251, p. 464-466.

Ramaseshan, S. and Ramachandran, G. N. (1953) Influence of mosaicity on the Bragg reflexion of polarized X-rays, Acta Crystallographica, vol. 6, pt. 4; p. 364-365.

Vand, Vladimir and Pepinsky, Ray (1953) The statistical approach to X-ray structure analysis, X-Ray and Crystal Analysis Laboratory, Department of Physics, Pennsylvania State University.

Zachariasen, W. H. (1946) The theory of X-ray diffraction in crystals. New York: John Wiley and Sons.

Zajac, A. (1958) Thermal motion in ice and heavy ice, Journal of Chemical Physics, vol. 29, p. 1324.

APPENDIX A. THERMISTOR BRIDGE.

For a great many applications, it is desirable to measure the temperature at a point and in so doing to alter the local temperature as little as possible. Usually when a high degree of accuracy is desired, it is relative accuracy which is of greatest importance. For such situations the thermistor bridge together with a low current null indicator constitute an inexpensive and very satisfactory instrument. However, the logarithmic temperature characteristic of the thermistor makes the calibration very non-linear and the sensitivity non-uniform.

The apparatus shown in Figures A1 and A2 is an inexpensive and simple instrument of high sensitivity which minimizes the difficulties mentioned above. It has now been in use for 3 yr and has proved to be a reliable and exceedingly convenient instrument. It has been used in the temperature range -80 to +20C, covered in four overlapping ranges. More can be added if desired.

The principle features to be emphasized are first the modified Wheatstone Bridge in which the slide wire resistor comprises the ratio arms. The non-linearity of this arrangement compensates in good measure for the non-linearity of the thermistor and results in S-shaped calibration curves (Fig. A3). Second, the driving voltage and the resistance in the bridge arm opposite the thermistor are different for each range. This provides roughly uniform temperature sensitivity on all scales as is also evident from Figure A3. Third, the transistor amplifier is balanced and is provided with a simple switching arrangement for zeroing both an open circuit and a short circuit. With this arrangement a 1 deg change in temperature corresponds to about four divisions on the dial which drives the slide wire potentiometer. This is a standard National Type N dial provided with a vernier which reads to 1/10 division. Thus the instrument is direct reading to about 0.02C. By using the deflection of the null indicator, changes of less than 0.01C can be measured.

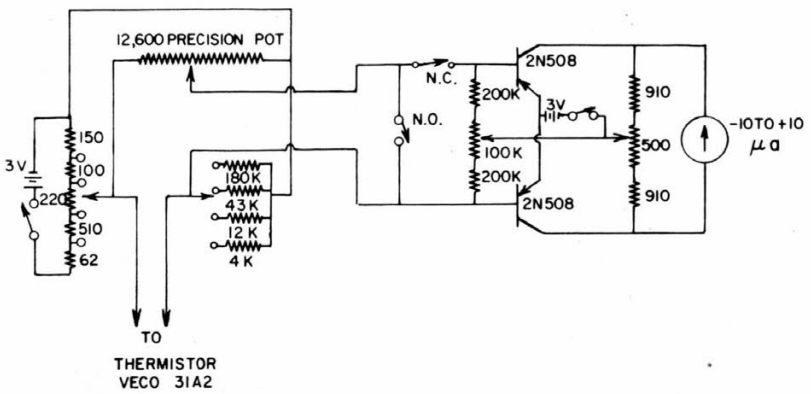

Figure A1. Circuit diagram of thermistor bridge.

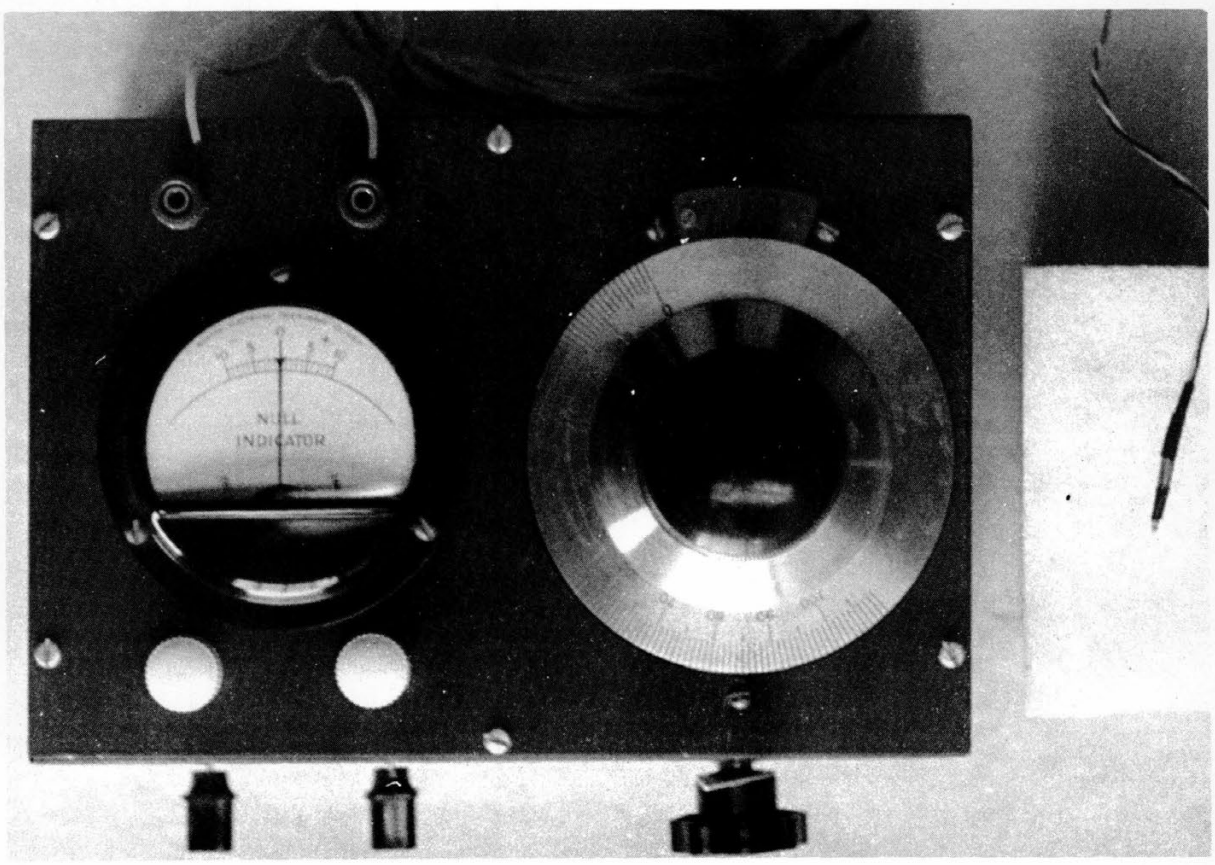

Figure A2. Photograph of thermistor bridge — completely self-contained except for thermistor.

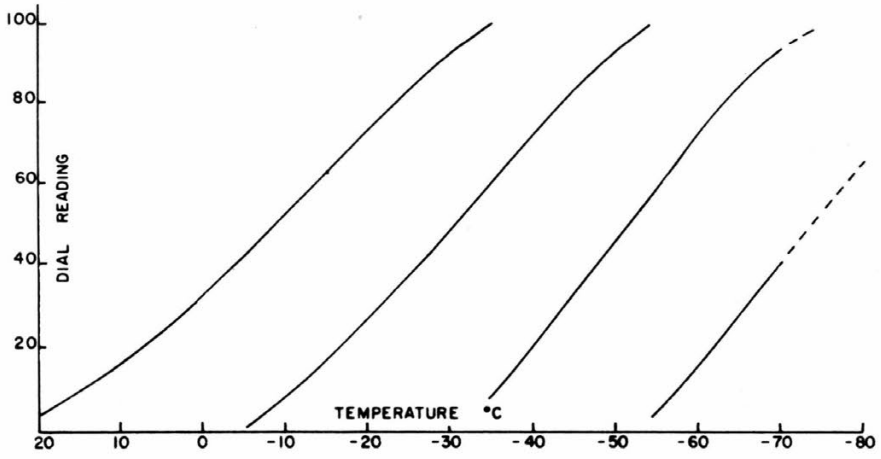

Figure A3. Typical calibration curves for thermistor bridge.